

Radiative Transport Equation in Rotated Reference Frames.

George Panasyuk, John C. Schotland

Department of Bioengineering, University of Pennsylvania, Philadelphia, PA 19104

Vadim A. Markel[†]

Department of Radiology, University of Pennsylvania, Philadelphia, PA 19104

Abstract. A novel method for solving the linear radiative transport equation in a three-dimensional macroscopically homogeneous random medium is proposed and illustrated with numerical examples. The method can be used with an arbitrary phase function $A(\hat{s}, \hat{s}')$ with the constraint that it depends only on the angle between the angular variables \hat{s} and \hat{s}' . This corresponds to spherically symmetrical (on average) random medium constituents. Boundary conditions are considered in the slab and half-space geometries. The approach developed in this paper is *spectral*. It allows one to expand the solution in analytical functions of angular and spatial variables to relatively high orders. The numerical coefficients of these expansion must be computed numerically. However, the computational complexity of this task is much smaller than in the standard method of spherical harmonics. The obtained solutions are especially convenient for solving inverse problems associated with the radiative transfer.

PACS numbers: 05.60.Cd, 87.57.Gg, 42.68.Ay, 95.30.Jx

Submitted to: *J. Phys. A: Math. Gen.*

[†] To whom correspondence should be addressed (vmarkel@mail.med.upenn.edu)

1. Introduction

1.1. Background

The contemporary mesoscopic-level theoretical description of multiple scattering of waves in random media is most often based on the linear radiative transport equation (RTE) [1]. Unfortunately, RTE is notoriously difficult to solve, even in the case of constant absorption and scattering coefficients. Known analytical solutions are few and of little practical importance. Yet, there is a growing need for accurate and computationally efficient solutions to the RTE in many fields of applied and fundamentals science. For example, in optical tomography of biological tissues [2, 3], the use of RTE is frequently required to accurately describe propagation of multiply scattered light. This is especially true in close proximity to sources or boundaries [4], or in regions with high absorption and low scattering [5, 6]. Accordingly, significant effort has been devoted to developing and refining efficient approximate and numerical methods for solving the RTE. In particular, recently explored approaches were based on the discrete ordinate method [7–9], cumulant expansion [10, 11], modifications of the Ambarzumian’s method [12, 13], and different levels of the P_L approximation [14, 15]. Algorithms for inversion of the RTE have also been proposed [16–19].

The discrete ordinate method (see [20] for detailed description) is, perhaps, the most common approach due to its simplicity and generality. An alternative to the discrete ordinate method is the method of spherical harmonics, often referred to as the P_L approximation in cases with special symmetry. This approach has the advantage of expressing the angular dependence of the specific intensity in a basis of analytical functions rather than in the completely local basis of discrete ordinates. However, when no special symmetry is present in the problem, the method of spherical harmonics can be practically carried out only to very low orders. In a recent paper [21], we have suggested a modification of the standard method of spherical harmonics. The modification is based on expanding the angular part of each Fourier component of the specific intensity in the basis of spherical functions defined in a reference frame whose z -axis is aligned with the direction of the Fourier vector \mathbf{k} . This approach resulted in significant mathematical simplifications and was referred to as *the modified method of spherical harmonics* in the original paper [21]. Here we find it more appropriate to call it *the method of rotated reference frames* (MRRF).

In Ref. [21], derivation of the RTE Green’s function by the MRRF was only briefly sketched and numerical examples were limited to a few simple cases with spherical symmetry. Here we give full mathematical detail of the derivation and discuss the mathematical properties of obtained solutions, derive plane-wave decomposition of the Green’s function, and generalize the MRRF to the case of planar boundaries. We also provide extensive numerical examples for cases with no special symmetry. The paper is organized as follows. In Section 1.2, we introduce the RTE and basic notations, and explain why the use of rotated reference frames is beneficial. In Section 2 we define spherical functions in rotated reference frames. In Section 3 we apply the MRRF

to derivation of the Green's function. In particular, the Green's function in Fourier representation is given in Section 3.1. Mathematical properties of obtained solutions are discussed in Section 3.2. Different representations for the Green's function in real space are given in Section 3.3. Plane-wave decomposition of the Green's function is derived in Section 3.4. In Section 3.5, we introduce evanescent modes of the homogeneous RTE. These modes are important mathematical constructs which can be used for solving the RTE in the presence of planar boundaries, as is shown in Section 3.6. In Section 4 contains numerical examples of applying the MRRF to calculating the Green's function in infinite space. Finally, Section 5 contains a discussion of obtained results.

1.2. RTE and the conventional method of spherical harmonics

The RTE describes propagation of the *specific intensity* $I(\mathbf{r}, \hat{\mathbf{s}})$ (at the spatial point \mathbf{r} and flowing in the direction specified by the unit vector $\hat{\mathbf{s}}$) in a medium characterized by the absorption and scattering coefficients μ_a and μ_s , and has the form

$$\hat{\mathbf{s}} \cdot \nabla I + (\mu_a + \mu_s)I = \mu_s \hat{A}I + \varepsilon . \quad (1)$$

Here $\varepsilon = \varepsilon(\mathbf{r}, \hat{\mathbf{s}})$ is the source and \hat{A} is the scattering operator defined by

$$\hat{A}I(\mathbf{r}, \hat{\mathbf{s}}) = \int A(\hat{\mathbf{s}}, \hat{\mathbf{s}}')I(\mathbf{r}, \hat{\mathbf{s}}')d^2\hat{\mathbf{s}}' . \quad (2)$$

The phase function $A(\hat{\mathbf{s}}, \hat{\mathbf{s}}')$ is normalized according to $\int A(\hat{\mathbf{s}}, \hat{\mathbf{s}}')d^2\hat{\mathbf{s}}' = 1$. We also assume that it depends only on the angle between $\hat{\mathbf{s}}$ and $\hat{\mathbf{s}}'$: $A(\hat{\mathbf{s}}, \hat{\mathbf{s}}') = f(\hat{\mathbf{s}} \cdot \hat{\mathbf{s}}')$. This fundamental assumption is often used and corresponds to scattering by spherically symmetrical particles.

In the conventional method of spherical harmonics, all angle-dependent quantities are expanded in the basis of spherical harmonics defined in the laboratory frame [22]:

$$I(\mathbf{r}, \hat{\mathbf{s}}) = \sum_{lm} I_{lm}(\mathbf{r})Y_{lm}(\hat{\mathbf{s}}) , \quad (3)$$

$$\varepsilon(\mathbf{r}, \hat{\mathbf{s}}) = \sum_{lm} \varepsilon_{lm}(\mathbf{r})Y_{lm}(\hat{\mathbf{s}}) , \quad (4)$$

$$A(\hat{\mathbf{s}}, \hat{\mathbf{s}}') = \sum_{lm} A_l Y_{lm}(\hat{\mathbf{s}})Y_{lm}^*(\hat{\mathbf{s}}') . \quad (5)$$

In particular, truncating the above series at $l = 1$ leads to the well-known diffusion approximation to the RTE [22]. In a more general case, substituting expansions (3)-(5) into the RTE (1), multiplying the resulting equations by $Y_{l'm'}^*(\hat{\mathbf{s}})$ and integrating over $\hat{\mathbf{s}}$ leads to the following system of equations for $I_{lm}(\mathbf{r})$:

$$\sum_{l'm'} \left[R_{lm,l'm'}^{(x)} \frac{\partial I_{l'm'}}{\partial x} + R_{lm,l'm'}^{(y)} \frac{\partial I_{l'm'}}{\partial y} + R_{lm,l'm'}^{(z)} \frac{\partial I_{l'm'}}{\partial z} \right] + \sigma_l I_{lm} = \varepsilon_{lm} , \quad (6)$$

where $R^{(\alpha)} = \int s_\alpha Y_{lm}^*(\hat{\mathbf{s}}) Y_{l'm'}(\hat{\mathbf{s}}) d^2\hat{\mathbf{s}}$ ($\alpha = x, y, z$) are matrices whose explicit form is given in Ref. [22] and

$$\sigma_l = \mu_a + \mu_s(1 - A_l). \quad (7)$$

This system of ordinary differential equations must be solved for $l = 0, 1, 2, \dots, l_{\max}$ and $m = -l, \dots, l$, where l_{\max} is the truncation order of the expansion (3)-(5).

In the classical text [22], Case and Zweifel wrote concerning the system of equations (6): “This rather awe-inspiring set of equations . . . has perhaps only academic interest” (p. 219). We note that the root of the difficulty is not that the matrices $R^{(\alpha)}$ are dense (in fact, they only couple coefficients with $m' = m$, $l' = l \pm 1$ for $\alpha = z$ and $m' = m \pm 1$, $l' = l \pm 1$ for $\alpha = x, y$) or non-commuting (in fact, it is easy to verify that all $R^{(\alpha)}$ commute). The difficulty is that these matrices operate on the spatial derivatives of I_{lm} taken along different directions. Thus, by viewing the set of three matrices $R^{(\alpha)}$ as a three-dimensional vector of matrices \mathbf{R} , and using the Fourier representation for I_{lm} , we can rewrite the term in the square bracket of (6) as $i\mathbf{k} \cdot \mathbf{R}_{lm,l'm'} I_{l'm'}(\mathbf{k})$. It can be seen that the matrix $\mathbf{k} \cdot \mathbf{R}$ depends explicitly on the direction and length of \mathbf{k} . (See similar formulation in Ref. [23].)

The method of rotated reference frames (MRRF), similarly to the conventional method of spherical harmonics, does not lead to separation of spatial and angular variables, which is impossible for the RTE. However, by choosing a different \mathbf{k} -dependent angular basis, we replace the dot product $\mathbf{k} \cdot \mathbf{R}$ by an expression of the type kR , where $k = |\mathbf{k}|$ is a scalar and R - a single \mathbf{k} -independent block-diagonal matrix. It is shown below that, given generalized eigenvectors and eigenvalues of R which must be computed numerically, the solution can be obtained in terms of analytical functions of spatial and angular variables. ‡

2. Spherical functions in rotated frames

The ordinary spherical harmonics $Y_{lm}(\theta, \varphi)$ are functions of two polar angles in a fixed (laboratory) reference frame. Equivalently, we can view them as functions of a unit vector, $\hat{\mathbf{s}}$. In this case, θ and φ are the polar angles of $\hat{\mathbf{s}}$ in the laboratory frame. In a more general case, both the orientation of the reference frame and the direction of $\hat{\mathbf{s}}$ can vary. We will need to define spherical functions of a unit vector $\hat{\mathbf{s}}$ in a reference frame whose z -axis coincides with the direction of a given unit vector $\hat{\mathbf{k}}$. Obviously, there are infinitely many such reference frames. To define one uniquely, it is sufficient to consider a rotation of the laboratory frame with the following three Euler angles: $\alpha = \varphi_{\hat{\mathbf{k}}}$, $\beta = \theta_{\hat{\mathbf{k}}}$ and $\gamma = 0$, where $\theta_{\hat{\mathbf{k}}}$ and $\varphi_{\hat{\mathbf{k}}}$ are the polar angles of $\hat{\mathbf{k}}$ in the laboratory frame. The

‡ In principle, it should be also possible to use the fact that all matrices $R^{(\alpha)}$ in (6) commute and, hence, have the same set of eigenvectors, to solve (6) by diagonalizing just one \mathbf{k} -independent matrix and analytically inverting the Fourier transform, and thus avoid the use of rotated reference frames. This approach has some advantages and difficulties associated with it, and to the best of our knowledge, has not been explored so far. If successful, it should lead to the same solutions as described below.

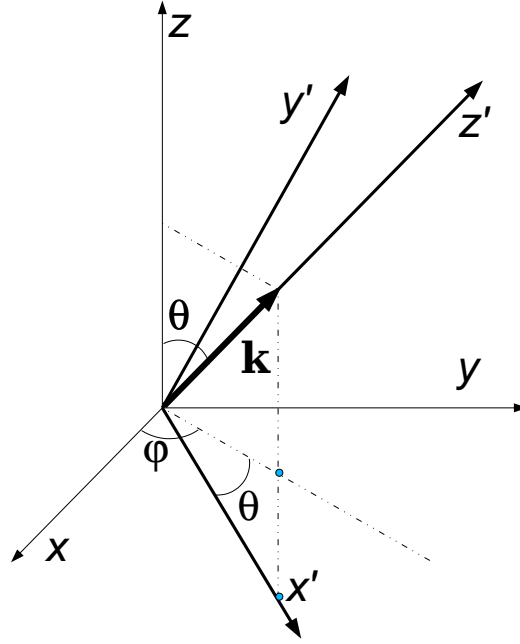


Figure 1. Illustration of the rotated reference frame

transformation from the laboratory frame (x, y, z) to the rotated frame (x', y', z') is illustrated in Fig. 1. We denote spherical functions of $\hat{\mathbf{s}}$ in the reference frame defined by the above transformation by $Y_{lm}(\hat{\mathbf{s}}; \hat{\mathbf{k}})$. They can be expressed as linear combinations of the spherical functions defined in the original (laboratory) frame according to

$$Y_{lm}(\hat{\mathbf{s}}; \hat{\mathbf{k}}) = \sum_{m'=-l}^l D_{m'm}^l(\varphi_{\hat{\mathbf{k}}}, \theta_{\hat{\mathbf{k}}}, 0) Y_{lm'}(\hat{\mathbf{s}}), \quad (8)$$

where

$$D_{mm'}^l(\alpha, \beta, \gamma) = \exp(-im\alpha) d_{mm'}^l(\beta) \exp(-im'\gamma) \quad (9)$$

are the Wigner D-functions; the explicit form of $d_{mm'}^l(\beta)$ is given, for example, in Ref. [24].

It is important to note that the expansion of the scattering kernel into the spherical functions $Y_{lm}(\hat{\mathbf{s}}; \hat{\mathbf{k}})$ is independent of the direction of $\hat{\mathbf{k}}$:

$$A(\hat{\mathbf{s}}, \hat{\mathbf{s}}') = \sum_{lm} A_l Y_{lm}(\hat{\mathbf{s}}; \hat{\mathbf{k}}) Y_{lm}^*(\hat{\mathbf{s}}'; \hat{\mathbf{k}}). \quad (10)$$

Here the expansion coefficients A_l are independent of $\hat{\mathbf{k}}$ and the same as in (5). This fact follows from the rotational invariance of the scalar product.

3. Theory

3.1. Green's function in the Fourier representation

By definition, the Green's function $G(\mathbf{r}, \hat{\mathbf{s}}; \mathbf{r}_0, \hat{\mathbf{s}}_0)$ satisfies RTE (1) with the delta-source $\varepsilon = \delta(\mathbf{r} - \mathbf{r}_0)\delta(\hat{\mathbf{s}} - \hat{\mathbf{s}}_0)$. We will refer to $\mathbf{r}_0, \hat{\mathbf{s}}_0$ and $\mathbf{r}, \hat{\mathbf{s}}$ as the location and direction of the source and detector, respectively. In infinite isotropic space, the Green's function can be written in the following general form:

$$G(\mathbf{r}, \hat{\mathbf{s}}; \mathbf{r}_0, \hat{\mathbf{s}}_0) = \sum_{lm, l'm'} \int \frac{d^3 k}{(2\pi)^3} \exp[i\mathbf{k} \cdot (\mathbf{r} - \mathbf{r}_0)] Y_{lm}(\hat{\mathbf{s}}; \hat{\mathbf{k}}) \langle lm|K(k)|l'm'\rangle Y_{l'm'}^*(\hat{\mathbf{s}}_0; \hat{\mathbf{k}}) . \quad (11)$$

Here $K(k)$ is an unknown operator. The reciprocity of the Green's function, $G(\mathbf{r}, \hat{\mathbf{s}}; \mathbf{r}_0, \hat{\mathbf{s}}_0) = G(\mathbf{r}_0, -\hat{\mathbf{s}}_0; \mathbf{r}, -\hat{\mathbf{s}})$, together with the fact that G is real, imply the following symmetry property of K : $\langle l'm'|K|lm\rangle = (-1)^{l+l'} \langle lm|K|l'm'\rangle^*$. This can be also written as $\mathcal{P}K^\dagger\mathcal{P} = K$, where \mathcal{P} is the coordinate inversion operator with matrix elements $\langle lm|\mathcal{P}|l'm'\rangle = (-1)^l \delta_{ll'} \delta_{mm'}$ and \dagger denotes Hermitian conjugation. Thus, it can be seen that K is not a Hermitian operator.

We note that the use of spherical functions defined in the locally rotated reference frames is the key element of the method described in this paper. Substituting (11) into (1) and using the orthogonality properties of spherical functions, we arrive at the following operator equation for $K(k)$:

$$(ikR + \Sigma)K(k) = 1 . \quad (12)$$

The matrices R and Σ are defined by

$$\begin{aligned} \langle lm|R|l'm'\rangle &= \int (\hat{\mathbf{s}} \cdot \hat{\mathbf{k}}) Y_{lm}^*(\hat{\mathbf{s}}; \hat{\mathbf{k}}) Y_{l'm'}(\hat{\mathbf{s}}; \hat{\mathbf{k}}) d^2\hat{\mathbf{s}} \\ &= \delta_{mm'} [b_{lm}\delta_{l'l-1} + b_{l+1,m}\delta_{l'l+1}] , \end{aligned} \quad (13)$$

$$b_{lm} = \sqrt{(l^2 - m^2)/(4l^2 - 1)} , \quad (14)$$

$$\langle lm|\Sigma|l'm'\rangle = \sigma_l \delta_{ll'} \delta_{mm'} , \quad (15)$$

where σ_l is given by (7). The formal solution to (12) can be written as

$$K(k) = S(1 + ikW)^{-1}S , \quad (16)$$

where $S = 1/\sqrt{\Sigma}$ and $W = SRS$. Note that $\langle lm|S|l'm'\rangle = \delta_{ll'} \delta_{mm'}/\sqrt{\sigma_l}$ exists because $\sigma_l > 0$, which follows from the inequalities $A_l \leq 1$ and $\mu_a > 0$ §. Similarly to R , W is a real symmetrical matrix. Therefore, we can use the spectral theorem to express

§ Purely scattering media with $\mu_a = 0$ can be considered separately.

$(1+ikW)^{-1}$ in terms of the eigenvectors and eigenvalues of W , $|\psi_\mu\rangle$ and λ_μ , respectively. This immediately leads to the following expression for $K(k)$:

$$K(k) = \sum_{\mu} \frac{S|\psi_\mu\rangle\langle\psi_\mu|S}{1+ik\lambda_\mu}, \quad (17)$$

Given the set of eigenvectors and eigenvalues, which can be found by numerical diagonalization of W , the above formula solves the problem in the Fourier space. Since the components of $|\psi_\mu\rangle$ in the $|lm\rangle$ basis are purely real, it can be seen that K is symmetrical. Combined with the property $\mathcal{P}K^\dagger\mathcal{P} = K$, this means that the even bands of K are purely real and odd bands purely imaginary.

3.2. Mathematical properties of the solution

3.2.1. Block structure of W

First, we note that W is block-diagonal: $\langle lm|W|l'm'\rangle = \delta_{mm'}\langle l|B(m)|l'\rangle$. Below, we will label different blocks $B(M)$ ($M = 0, \pm 1, \pm 2, \dots$) by the capital letter M . The matrix elements of $B(M)$ are given by

$$\langle l|B(M)|l'\rangle = \beta_l(M)\delta_{l'=l-1} + \beta_{l+1}(M)\delta_{l'=l+1}, \quad l, l' \geq |M|, \quad (18)$$

$$\beta_l(M) = b_{lM}/\sqrt{\sigma_l\sigma_{l-1}}. \quad (19)$$

Obviously, to find all eigenvalues and eigenvectors of W , it is sufficient to diagonalize each block separately. This task is further simplified because all blocks $B(M)$ are tridiagonal. We denote eigenvectors of a block $B(M)$ by $|\phi_n(M)\rangle$. Then the eigenvector of the full matrix W with the same eigenvalue is obtained according to

$$\langle lm|\psi_{Mn}\rangle = \delta_{mM}\langle l|\phi_n(M)\rangle. \quad (20)$$

The corresponding eigenvector is denoted by λ_{Mn} , where we have introduced a composite index $\mu = (M, n)$. Note that $B(M) = B(-M)$.

3.2.2. Symmetry properties of the eigenvectors

The property $\mathcal{P}K^\dagger\mathcal{P} = K$ and Eq. (16) imply that $\mathcal{P}W\mathcal{P} = -W$. Thus, W is odd with respect to coordinate inversion. In particular, if $|\psi\rangle$ is an eigenvector of W with the eigenvalue λ , then $|\tilde{\psi}\rangle = \mathcal{P}|\psi\rangle$ is also an eigenvector of W but with an eigenvalue of the opposite sign, $\tilde{\lambda} = -\lambda$. The complete set of eigenvectors $\{|\psi_\mu\rangle : \mu \in \Omega\}$, where Ω is the set of all values of the index μ , can then be equivalently rewritten as $\{|\psi_\mu\rangle, |\tilde{\psi}_\mu\rangle : \mu \in \Omega^+\}$, where Ω^+ is the set of indices μ that correspond to positive eigenvalues λ_μ . The set of indices that correspond to negative eigenvalues can be denoted as Ω^- ; then $\Omega = \Omega^+ \cup \Omega^-$ and $\Omega^+ \cap \Omega^- = 0$.

Using these properties, one can transform the summation over all values of μ in (17) to summation over $\mu \in \Omega^+$ (such sums will be denoted as \sum'_μ below). This fact facilitates the inverse Fourier transformation (see Appendix A) and solution of the boundary-value problem discussed in Section 3.6.

3.2.3. Continuous and discrete spectra

Third, the eigenvalues λ_μ can belong either to discrete or continuous spectrum. It is easy to see that the spectrum is continuous for $|\lambda| < 1/\mu_t$, where $\mu_t = \mu_a + \mu_s$, and discrete for $|\lambda| > 1/\mu_t$. Indeed, consider the three-point recurrence relation that follows from the equation $W|\psi\rangle = \lambda|\psi\rangle$:

$$\beta_l(m)\langle l-1, m|\psi\rangle + \beta_{l+1}(m)\langle l+1, m|\psi\rangle = \lambda\langle lm|\psi\rangle, \quad l \geq |m|. \quad (21)$$

In general, it has two types of solutions: polynomial and exponential. Consider the asymptotic properties of these solutions. In the limit $l \rightarrow \infty$ we have $A_l \rightarrow 0$, $\sigma_l \rightarrow \mu_t$, $b_{lm} \rightarrow 1/2$ and $\beta_l(m) \rightarrow 1/2\mu_t$. The recurrence relation then becomes:

$$\langle l-1, m|\psi\rangle + \langle l+1, m|\psi\rangle = 2\mu_t\lambda\langle lm|\psi\rangle. \quad (22)$$

The polynomial solutions have the asymptotic form $\langle lm|\psi\rangle = P_l^m(\lambda\mu_t)$, where $P_l^m(x)$ are general orthogonal polynomials of degree l (not to be confused with the associated Legendre functions which solve the recurrence (21) in the particular case $\mu_s = 0$). In order for this solution to be an eigenvector of W , it must be bounded. Obviously, this requirement is equivalent to $|\lambda\mu_t| \leq 1$. Thus, for every $\lambda \in [-1/\mu_t, 1/\mu_t]$, there is a polynomial solution to the three-term recurrence relation that is an eigenvector of W .

For λ outside of the interval $[-1/\mu_t, 1/\mu_t]$, polynomial solutions are unbounded and, therefore, can not be eigenvectors of W . We then consider exponential solutions which behave asymptotically as $\langle lm|\psi\rangle = (\pm 1)^l \exp(-pl)$ where p satisfies the equation $\cosh(p) = \pm\mu_t\lambda$. In order for this solution to be an eigenvector of W , p must be positive. But the above equation has positive roots only when $|\lambda| \geq 1/\mu_t$. Note that the exponentially decaying eigenvectors have a finite L_2 norm, and, hence, belong to the discrete spectrum. Further bounds of the discrete spectrum can be inferred from the Gershgorin theorem, which states that, for a fixed M , $|\lambda_{Mn}| \leq r_M = \max_{l \geq |M|} [\beta_l(M) + \beta_{l+1}(M)]$. It can be easily verified that $r_0 = 4/\sqrt{3}\mu_a$ and $r_M = 1/\mu_a$ for $|M| > 0$.

In numerical computations, the infinite-dimensional matrix W must be truncated and the continuous spectrum of W approximated by a discrete spectrum. In this paper we treat all eigenvectors as discrete. Thus, for example, expression (17) contains only a sum over discrete modes, although, theoretically, summation over the continuous part of the spectrum must be expressed as an integral. Note that an expression involving only discrete spectra avails itself more readily to a numerical implementation.

3.3. Green's function in real space

The dependence of solution (17) on \mathbf{k} is analytical. This allows us to obtain the Green's function the coordinate representation by analytical Fourier transform. We substitute (17) into the ansatz (11) and express the spherical functions $Y_{lm}(\hat{\mathbf{s}}; \hat{\mathbf{k}})$ and $Y_{l'm'}(\hat{\mathbf{s}}_0; \hat{\mathbf{k}})$ in terms of spherical functions defined in the laboratory frame whose z -axis direction is

given by a unit vector $\hat{\mathbf{z}}$ according to (8),(9). The direction of the x - and y -axes of the laboratory frame is arbitrary. This leads to the following expression:

$$G(\mathbf{r}, \hat{\mathbf{s}}; \mathbf{r}_0, \hat{\mathbf{s}}_0) = \sum_{lm} \sum_{l'm'} Y_{lm}(\hat{\mathbf{s}}; \hat{\mathbf{z}}) \langle lm | \chi(\mathbf{r} - \mathbf{r}_0; \hat{\mathbf{z}}) | l'm' \rangle Y_{l'm'}^*(\hat{\mathbf{s}}_0; \hat{\mathbf{z}}) , \quad (23)$$

where

$$\chi(\mathbf{r}; \hat{\mathbf{z}}) = \int \frac{d^3\mathbf{k}}{(2\pi)^3} \exp(i\mathbf{k} \cdot \mathbf{r}) \mathcal{D}(\hat{\mathbf{k}}; \hat{\mathbf{z}}) K(k) \mathcal{D}^\dagger(\hat{\mathbf{k}}; \hat{\mathbf{z}}) \quad (24)$$

Here $\mathcal{D}(\hat{\mathbf{k}}; \hat{\mathbf{z}}) = \exp(-i\varphi_{\hat{\mathbf{k}}} J_z - i\theta_{\hat{\mathbf{k}}} J_y)$ is the rotation operator whose matrix elements are given by the Wigner functions, $\langle lm | \mathcal{D}(\hat{\mathbf{k}}; \hat{\mathbf{z}}) | l'm' \rangle = \delta_{ll'} D_{mm'}^l(\varphi_{\hat{\mathbf{k}}}, \theta_{\hat{\mathbf{k}}}, 0)$, $\varphi_{\hat{\mathbf{k}}}$ and $\theta_{\hat{\mathbf{k}}}$ are the polar angles of \mathbf{k} in the laboratory frame, and \mathbf{J} is the operator of angular momentum. We note that operators \mathcal{D} are unitary and, hence, normal: $\mathcal{D}^{-1} = \mathcal{D}^\dagger$. However, \mathcal{D} does not commute with K . The fundamental simplification obtained by the MRRF is that \mathcal{D} is known analytically while K has a simple form given by (17). In particular, given numerical values of $|\psi_\mu\rangle$ and λ_μ , the dependence of $K(k)$ on k is also known analytically.

Below, we consider two different cases. In the first case, the direction of the laboratory frame z -axis coincides with the direction from the source to the detector, namely, $\hat{\mathbf{z}} = (\mathbf{r} - \mathbf{r}_0)/|\mathbf{r} - \mathbf{r}_0|$. This choice of the angular basis is convenient when the source and the detector are always placed on the same line, irrespectively of the directions $\hat{\mathbf{s}}$ and $\hat{\mathbf{s}}_0$. In the second case, we choose $\hat{\mathbf{z}} = \hat{\mathbf{s}}_0$. This approach is useful when the source is scanned, e.g., over a two-dimensional plane, but its direction $\hat{\mathbf{s}}_0$ is fixed. This situation is typical for optical tomography in a slab geometry. The integral (24) for the two cases is evaluated in Appendix A. The result is, in the first case:

$$\begin{aligned} \langle lm | \chi(\mathbf{r}; \hat{\mathbf{r}}) | l'm' \rangle &= \frac{\delta_{mm'}}{2\pi \sqrt{\sigma_l \sigma_{l'}}} \sum_{M=-\bar{l}}^{\bar{l}} (-1)^M \sum_{j=0}^{\bar{l}} C_{l,M,l',-M}^{l-l'+2j,0} C_{l,m,l',-m}^{l-l'+2j,0} \\ &\times \sum_{\mu}' \frac{\langle lM | \psi_\mu \rangle \langle \psi_\mu | l'M \rangle}{\lambda_\mu^3} k_{|l-l'+2j} \left(\frac{R}{\lambda_\mu} \right) , \end{aligned} \quad (25)$$

Here $\bar{l} = \min(l, l')$, $k_n(x) = -i^n h_n^{(1)}(ix)$ is the modified spherical Bessel function of the first kind (defined without the $\pi/2$ factor), $C_{j_1 m_1 j_2 m_2}^{j_3 m_3}$ are the Clebsch-Gordan coefficients and \sum' denotes summation over only such indices μ that correspond to positive eigenvalues λ_μ . It can be seen that $\chi(\mathbf{r}; \hat{\mathbf{r}})$ is diagonal in m and m' , which corresponds to the invariance of the Green's function with respect to a simultaneous rotations of vectors $\hat{\mathbf{s}}$ and $\hat{\mathbf{s}}_0$ around the line connecting the source and the detector. Equation (25) can be further simplified by expressing the eigenvectors $|\psi_\mu\rangle$ in terms of the eigenvectors $|\phi_n(m)\rangle$ of smaller blocks $B(m)$ as discussed in Section 3.2.1. This result, as well as a number of special cases, were given in Ref. [21] and are not repeated here.

In the case $\hat{\mathbf{z}} = \hat{\mathbf{s}}_0$, expression (23) contains only matrix elements of $\chi(\mathbf{r}; \hat{\mathbf{s}}_0)$ with $m' = 0$. This follows from the fact that $Y_{l'm'}(\hat{\mathbf{s}}_0; \hat{\mathbf{s}}_0) = \delta_{m'0} \sqrt{(2l'+1)/4\pi}$. The corresponding expression for the matrix elements of $\chi(\mathbf{r}; \hat{\mathbf{s}}_0)$ is

$$\begin{aligned} \langle lm|\chi(\mathbf{r}; \hat{\mathbf{s}}_0)|l'0\rangle &= \frac{1}{2\pi\sqrt{\sigma_l\sigma_{l'}}} \sum_{M=-\bar{l}}^{\bar{l}} (-1)^M \sum_{j=0}^{\bar{l}} \sqrt{\frac{4\pi}{2[|l-l'|+2j]+1}} Y_{|l-l'+2j,m}^*(\hat{\mathbf{r}}; \hat{\mathbf{s}}_0) \\ &\times C_{l,M,l',-M}^{|l-l'+2j,0} C_{l,m,l',0}^{|l-l'+2j,m} \sum_{\mu} \frac{\langle lM|\psi_{\mu}\rangle \langle \psi_{\mu}|l'M\rangle}{\lambda_{\mu}^3} k_{|l-l'+2j} \left(\frac{R}{\lambda_{\mu}}\right). \end{aligned} \quad (26)$$

Derivation of the above result is analogous to that for $\chi(\mathbf{r}; \hat{\mathbf{r}})$; see Appendix A for details.

3.4. Plane-wave decomposition of the Green's function

Having in mind further application of the MRRF to solving boundary value problems, we derive the plane-wave decomposition of the Green's function. The latter is defined by the two-dimensional Fourier integral

$$\begin{aligned} G(\mathbf{r}, \hat{\mathbf{s}}; \mathbf{r}_0, \hat{\mathbf{s}}_0) &= \sum_{lm} \sum_{l'm'} \int \frac{d^2q}{(2\pi)^2} \exp[i\mathbf{q} \cdot (\boldsymbol{\rho} - \boldsymbol{\rho}_0)] \\ &\times Y_{lm}(\hat{\mathbf{s}}; \hat{\mathbf{z}}) \langle lm|\kappa(\mathbf{q}; z - z_0)|l'm'\rangle Y_{l'm'}^*(\hat{\mathbf{s}}_0; \hat{\mathbf{z}}). \end{aligned} \quad (27)$$

Here $\hat{\mathbf{z}}$ is a selected direction in space which coincides with the z -axis of the laboratory frame, $\boldsymbol{\rho}$ is a two-dimensional vector in the $x - y$ plane ($\mathbf{r} = \boldsymbol{\rho} + z\hat{\mathbf{z}}$ and $\boldsymbol{\rho} \cdot \hat{\mathbf{z}} = 0$) and the direction of x - and y -axes is arbitrary. By comparing the above expression to (24), we find that

$$\kappa(\mathbf{q}; z) = \int_{-\infty}^{\infty} \frac{dk_z}{2\pi} \exp(ik_z z) \mathcal{D}(\mathbf{q} + \hat{\mathbf{z}}k_z; \hat{\mathbf{z}}) K\left(\sqrt{q^2 + k_z^2}\right) \mathcal{D}^\dagger(\mathbf{q} + \hat{\mathbf{z}}k_z; \hat{\mathbf{z}}). \quad (28)$$

Here $\mathcal{D}(\mathbf{q} + \hat{\mathbf{z}}k_z; \hat{\mathbf{z}})$ should be understood as a function of the polar angles of the vector $\mathbf{k} = \mathbf{q} + \hat{\mathbf{z}}k_z$ in the laboratory frame. The latter are defined by

$$\cos\theta = k_z/\sqrt{q^2 + k_z^2}, \quad \sin\theta = q/\sqrt{q^2 + k_z^2}. \quad (29)$$

Integral (28) can be evaluated analytically. The following expression for the matrix elements of $\kappa(\mathbf{q}; z)$ is derived in Appendix B:

$$\begin{aligned} \langle lm|\kappa(\mathbf{q}; z)|l'm'\rangle &= \frac{\exp[-i(m-m')\varphi_{\mathbf{q}}]}{\sqrt{\sigma_l\sigma_{l'}}} [\text{sgn}(z)]^{l+l'+m+m'} \sum_{m_1=-l}^l \sum_{m_2=-l'}^{l'} \sum_{\mu} \\ &\times d_{mm_1}^l[i\tau(q\lambda_{\mu})] \langle lm_1|\psi_{\mu}\rangle \frac{\exp[-Q_{\mu}(q)|z|]}{\lambda_{\mu}^2 Q_{\mu}(q)} \langle \psi_{\mu}|l'm_2\rangle d_{m'm_2}^{l'}[i\tau(q\lambda_{\mu})], \end{aligned} \quad (30)$$

where

$$Q_{\mu}(q) = \sqrt{q^2 + 1/\lambda_{\mu}^2}, \quad (31)$$

the complex angles $i\tau(x)$ are defined by the relations

$$\cos[i\tau(x)] = \sqrt{1+x^2}, \quad \sin[i\tau(x)] = -ix, \quad (32)$$

and the angle $\varphi_{\hat{\mathbf{q}}}$ is the polar angle of the two-dimensional vector \mathbf{q} in the $x - y$ plane. The Wigner d-functions $d_{mm'}^l(i\tau)$ in the above expression are algebraic functions of $\cos(i\tau)$ and $\sin(i\tau)$ (an explicit expression in terms of Jacobi polynomials is given in Appendix B). An expression for $\kappa(\mathbf{q}; z)$ in terms of block eigenvectors $|\phi_n(M)\rangle$ which were introduced in Section 3.2.1 is also given in Appendix B. Here we note some of the symmetry properties of the matrices $\kappa(\mathbf{q}; z)$. Under inversion of the z -axis, we have $\kappa(\mathbf{q}, -z) = \mathcal{P}_z \kappa(\mathbf{q}, z) \mathcal{P}_z$, or, in components,

$$\langle lm | \kappa(\mathbf{q}; -z) | l'm' \rangle = (-1)^{l+l'+m+m'} \langle lm | \kappa(\mathbf{q}; z) | l'm' \rangle . \quad (33)$$

Simultaneous inversion of the x - and y -axes (or, equivalently, rotation around the z -axis by the angle π) is expressed as $\kappa(-\mathbf{q}, z) = \mathcal{P}_{xy} \kappa(\mathbf{q}, z) \mathcal{P}_{xy}$, or, in components,

$$\langle lm | \kappa(-\mathbf{q}; z) | l'm' \rangle = (-1)^{m+m'} \langle lm | \kappa(\mathbf{q}; z) | l'm' \rangle . \quad (34)$$

We also note some particular cases of expressions (27) and (30). First, consider the case $\hat{\mathbf{s}} = \hat{\mathbf{s}}_0 = \hat{\mathbf{z}}$. This corresponds to the source and detector being oriented perpendicular to a slab. We then use $Y_{lm}(\hat{\mathbf{z}}; \hat{\mathbf{z}}) = \delta_{m0} \sqrt{(2l+1)/4\pi}$ to obtain

$$G(\mathbf{r}, \hat{\mathbf{z}}; \mathbf{r}_0, \hat{\mathbf{z}}) = \sum_{l, l'=0}^{\infty} \frac{\sqrt{(2l+1)(2l'+1)}}{4\pi} \int \frac{d^2q}{(2\pi)^2} \exp[i\mathbf{q} \cdot (\boldsymbol{\rho} - \boldsymbol{\rho}_0)] \langle l0 | \kappa(\mathbf{q}; z - z_0) | l'0 \rangle . \quad (35)$$

With the use of identity (A.12) given below, $\langle l0 | \kappa(\mathbf{q}; z) | l'0 \rangle$ can be expressed in terms of the associated Legendre functions of the first kind $P_l^m(x)$ as

$$\begin{aligned} \langle l0 | \kappa(\mathbf{q}; z) | l'0 \rangle &= \frac{[\text{sgn}(z)]^{l+l'}}{\sqrt{\sigma_l \sigma_{l'}}} \sum_{m_1=-l}^l \sum_{m_2=-l'}^{l'} \sqrt{\frac{(l-m_1)!(l'-m_2)!}{(l+m_1)!(l'+m_2)!}} \sum_{\mu} P_l^{m_1}[\lambda_{\mu} Q_{\mu}(q)] \\ &\times \langle lm_1 | \psi_{\mu} \rangle \frac{\exp[-Q_{\mu}(q)|z|]}{\lambda_{\mu}} \langle \psi_{\mu} | l'm_2 \rangle P_{l'}^{m_2}[\lambda_{\mu} Q_{\mu}(q)] . \end{aligned} \quad (36)$$

Next, consider the case $\mathbf{q} = 0$. Operator $\kappa(0; z)$ describes one-dimensional propagation due to a planar source. We use $d_{mm'}^l(0) = \delta_{mm'}$ to obtain

$$\langle lm | \kappa(0; z) | l'm' \rangle = \frac{\delta_{mm'} [\text{sgn}(z)]^{l+l'}}{\sqrt{\sigma_l \sigma_{l'}}} \sum_{\mu} \langle lm | \psi_{\mu} \rangle \frac{\exp(-|z|/\lambda_{\mu})}{\lambda_{\mu}} \langle \psi_{\mu} | l'm' \rangle . \quad (37)$$

3.5. Plane wave and evanescent modes for the RTE

Above we considered solutions to the inhomogeneous RTE. However, solution of boundary value problems requires the knowledge of the general solution to the homogeneous equation. General solutions to RTE (1) with zero right-hand side can be written as

$$I_{\hat{\mathbf{k}}, M, n}(\mathbf{r}, \hat{\mathbf{s}}) = \exp\left(\frac{-\hat{\mathbf{k}} \cdot \mathbf{r}}{\lambda_{Mn}}\right) \sum_{lm} Y_{lm}(\hat{\mathbf{s}}; \hat{\mathbf{z}}) \frac{\exp(-im\varphi_{\hat{\mathbf{k}}})}{\sqrt{\sigma_l}} d_{mM}^l(\theta_{\hat{\mathbf{k}}}) \langle l | \phi_n(M) \rangle . \quad (38)$$

Here it is more convenient to use the notations for block eigenvectors $|\phi_n(M)\rangle$ which were introduced in Section 3.2.1. The modes are labeled by the unit vector $\hat{\mathbf{k}}$ ($\hat{\mathbf{k}} \cdot \hat{\mathbf{k}} = 1$) whose polar angles in the laboratory frame are $\theta_{\hat{\mathbf{k}}}$ and $\varphi_{\hat{\mathbf{k}}}$ and by the composite index $\mu = (M, n)$. We note that it is sufficient to consider only modes with positive eigenvalues λ_{Mn} ($\mu \in \Omega^+$; see Section 3.2.2) due to the obvious symmetry $I_{-\hat{\mathbf{k}}, -M, n}(-\mathbf{r}, \hat{\mathbf{s}}) = I_{\hat{\mathbf{k}}, M, n}(\mathbf{r}, \hat{\mathbf{s}})$.

However, the modes (38) with purely real vector $\hat{\mathbf{k}}$ can not be used to construct a solution to a boundary value problem in a half-space or in a slab. This is because each of these modes is exponentially growing in the direction of $-\hat{\mathbf{k}}$. Therefore, it is necessary to define *evanescent* modes with complex-valued vectors $\hat{\mathbf{k}}$. These modes are oscillatory in the $x-y$ plane and exponentially decaying (or growing) in the z -direction. Namely, let

$$\hat{\mathbf{k}} = -i\lambda_{Mn}\mathbf{q} \pm \hat{\mathbf{z}}\lambda_{Mn}Q_{Mn}(q), \quad (39)$$

where $\mathbf{q} \cdot \hat{\mathbf{z}} = 0$. The polar angles of $\hat{\mathbf{k}}$ are defined as follows: $\varphi_{\hat{\mathbf{k}}} = \varphi_{\hat{\mathbf{q}}}$, $\cos(\theta_{\hat{\mathbf{k}}}) = \hat{\mathbf{k}} \cdot \hat{\mathbf{z}} = \pm\lambda_{Mn}Q_{Mn}(q)$ and $\sin(\theta_{\hat{\mathbf{k}}}) = \hat{\mathbf{k}} \cdot \hat{\mathbf{q}} = -iq\lambda_{Mn}$. Thus, we can write $\theta_{\hat{\mathbf{k}}} = i\tau(q\lambda_{Mn})$, where the sine and cosine of the complex angle $i\tau(x)$ are given by (32). This gives rise to two kinds of evanescent modes:

$$I_{\mathbf{q}, M, n}^{(+)}(\mathbf{r}, \hat{\mathbf{s}}) = \exp[i\mathbf{q} \cdot \boldsymbol{\rho} - Q_{\mu}(q)z] \sum_{lm} Y_{lm}(\hat{\mathbf{s}}; \hat{\mathbf{z}}) \frac{\exp(-im\varphi_{\hat{\mathbf{q}}})}{\sqrt{\sigma_l}} \\ \times d_{mM}^l[i\tau(q\lambda_{Mn})] \langle l | \phi_n(M) \rangle, \quad (40)$$

$$I_{\mathbf{q}, M, n}^{(-)}(\mathbf{r}, \hat{\mathbf{s}}) = (-1)^M \exp[i\mathbf{q} \cdot \boldsymbol{\rho} + Q_{\mu}(q)z] \sum_{lm} Y_{lm}(\hat{\mathbf{s}}; \hat{\mathbf{z}}) \frac{\exp(-im\varphi_{\hat{\mathbf{q}}})}{\sqrt{\sigma_l}} \\ \times (-1)^{l+m} d_{m, -M}^l[i\tau(q\lambda_{Mn})] \langle l | \phi_n(M) \rangle. \quad (41)$$

Here we have used the symmetry properties of $d_{mM}^l(\theta)$ under the transformation $\theta \rightarrow \pi - \theta$ (which corresponds to change of sign of the factor $\cos(\theta)$); hence the additional phase factor $(-1)^{l+m}$ and the different sign of the index M in (41). The phase factor $(-1)^M$ is introduced for convenience.

The plane-wave decomposition (30) can be equivalently rewritten as an expansion in terms of evanescent waves:

$$G(\mathbf{r}, \hat{\mathbf{s}}; \mathbf{r}_0, \hat{\mathbf{s}}_0) = \sum_{\mu}' \int \frac{d^2q}{(2\pi)^2} V_{\mathbf{q}, \mu} I_{\mathbf{q}, \mu}^{(\pm)}(\mathbf{r}, \hat{\mathbf{s}}) I_{-\mathbf{q}, \mu}^{(\mp)}(\mathbf{r}_0, -\hat{\mathbf{s}}_0), \quad (42)$$

where

$$V_{\mathbf{q}, \mu} = \frac{1}{\lambda_{\mu}^2 Q_{\mu}(q)} \quad (43)$$

and the upper signs must be selected if $z > z_0$ while the lower signs are selected if $z < z_0$. It can be easily verified that the expression (42) is reciprocal.

Now we make the following observation. Evanescent waves propagating in different directions can not, in principle, have identical angular dependence. In particular, by

analyzing only the angular dependence of specific intensity in the plane $z = 0$ (in infinite space), it is possible to tell if this intensity was produced by sources located to the left of the observation plane (in the region $z < 0$), or to the right. To demonstrate this point, we introduce vectors $|\eta_\mu(q)\rangle = |\eta_{Mn}(q)\rangle$ with components $\langle lm|\eta_{Mn}(q)\rangle = d_{mM}^l[i\tau(q\lambda_{Mn})]\langle l|\phi_n(M)\rangle$ and a set of vectors obtained from $|\eta_\mu(q)\rangle$ by coordinate inversion: $|\tilde{\eta}_\mu(q)\rangle = \mathcal{P}|\eta_\mu(q)\rangle$. The evanescent modes (40),(41) can be written as

$$I_{\mathbf{q},\mu}^{(+)}(\mathbf{r}, \hat{\mathbf{s}}) = \exp[i\mathbf{q} \cdot \boldsymbol{\rho} - Q_\mu(q)z] \sum_{lm} Y_{lm}(\hat{\mathbf{s}}; \hat{\mathbf{z}}) \langle lm|\mathcal{A}(\hat{\mathbf{q}})|\eta_\mu(q)\rangle, \quad (44)$$

$$I_{\mathbf{q},\mu}^{(-)}(\mathbf{r}, \hat{\mathbf{s}}) = \exp[i\mathbf{q} \cdot \boldsymbol{\rho} + Q_\mu(q)z] \sum_{lm} Y_{lm}^*(\hat{\mathbf{s}}; \hat{\mathbf{z}}) \langle lm|\mathcal{A}^\dagger(-\hat{\mathbf{q}})|\tilde{\eta}_\mu(q)\rangle, \quad (45)$$

$$\langle lm|\mathcal{A}(\hat{\mathbf{q}})|l'm'\rangle = \delta_{ll'}\delta_{mm'} \exp(-im\varphi_{\hat{\mathbf{q}}})/\sqrt{\sigma_l} \quad (46)$$

Here $\mathcal{A}(\hat{\mathbf{q}})$ is a diagonal matrix. Note that $\mathcal{A}(\hat{\mathbf{q}})$ depends only on the direction of the real vector \mathbf{q} , while $|\eta_\mu(q)\rangle$ depends only on its length. In the case $q = 0$ we have $|\eta_\mu(0)\rangle = |\psi_\mu\rangle$ and $|\tilde{\eta}_\mu(0)\rangle = |\tilde{\psi}_\mu\rangle$. Thus, the set $\{|\eta_\mu(0)\rangle, |\tilde{\eta}_\mu(0)\rangle\}$ forms an orthonormal basis in \mathcal{H} . In the case $q \neq 0$, the vectors $\{|\eta_\mu(q)\rangle, |\tilde{\eta}_\mu(q)\rangle\}$ are no longer orthonormal. However, we believe on physical grounds that they still form a basis of \mathcal{H} ||. Then there exists a *dual basis* $\{|\zeta_\mu(q)\rangle, |\tilde{\zeta}_\mu(q)\rangle\}$ such that $\langle \zeta_\mu(q)|\eta_\nu(q)\rangle = \delta_{\mu\nu}$, $\langle \tilde{\zeta}_\mu(q)|\tilde{\eta}_\nu(q)\rangle = \delta_{\mu\nu}$ and $\langle \tilde{\zeta}_\mu(q)|\eta_\nu(q)\rangle = \langle \zeta_\mu(q)|\tilde{\eta}_\nu(q)\rangle = 0$.

Now assume that we have measured the specific intensity in the plane $z = 0$. Denote the two-dimensional Fourier transform of this function with respect to x and y by $I_0(\mathbf{q}, \hat{\mathbf{s}}) = \sum_{lm} I_{lm}(\mathbf{q})Y_{lm}(\hat{\mathbf{s}}; \hat{\mathbf{z}})$. The expansion coefficients $I_{lm}(\mathbf{q})$ are elements of a vector $|I(\mathbf{q})\rangle$. For every value of \mathbf{q} , we can form a vector $\mathcal{A}^{-1}(\hat{\mathbf{q}})|I(\mathbf{q})\rangle$, since $\mathcal{A}(\hat{\mathbf{q}})$ is easily invertible. If the sources are located to the left of the measurement plane, then $\langle \tilde{\zeta}_\mu(q)|\mathcal{A}^{-1}(\hat{\mathbf{q}})|I(\mathbf{q})\rangle = 0$ for every $\mu \in \Omega^+$. In other words, the projection of $\mathcal{A}^{-1}(\hat{\mathbf{q}})|I(\mathbf{q})\rangle$ onto the dual subspace spanned by $|\zeta_\mu(q)\rangle$ is equal to zero. Analogously, if the sources are located to the right of the observation plane, $\langle \zeta_\mu(q)|\mathcal{A}^{-1}(\hat{\mathbf{q}})|I(\mathbf{q})\rangle = 0$. Since the projection of a nonzero vector onto both subspaces can not be simultaneously zero, the angular dependence of the specific intensity in the plane $z = 0$ carries information about the location of the source with respect to this plane. We emphasize that this analysis is only valid in the absence of boundaries.

3.6. Boundary value problem

Any solution to the RTE in a half-space or in a slab can be constructed as an expansion over modes (44),(45) with indices μ corresponding to only positive eigenvalues λ_μ . This fact is crucial for application of the MRRF to the boundary value problem, which in the radiative transport theory is formulated in the *half-range* of the angular variable.

|| We do not have a direct proof of this statement. However, in the opposite case, the boundary value problem would not be uniquely solvable.

Now we demonstrate how it can be used to construct a solution to the boundary value problem posed on one or two planar interfaces.

3.6.1. External source incident on a half-space

Consider RTE in the half-space $z > 0$. In this Section we assume that there are no *internal sources* in the medium. The boundary condition at the planar interface $z = 0$ is formulated as

$$I_0(\boldsymbol{\rho}, \hat{\mathbf{s}}) = I_{\text{inc}}(\boldsymbol{\rho}, \hat{\mathbf{s}}) , \quad \text{if } \hat{\mathbf{s}} \cdot \hat{\mathbf{z}} > 0 . \quad (47)$$

Here $I_0(\boldsymbol{\rho}, \hat{\mathbf{s}})$ is the specific intensity evaluated at $z = 0$ and $I_{\text{inc}}(\boldsymbol{\rho}, \hat{\mathbf{s}})$ is the intensity incident from vacuum (the external source). The boundary condition (47) is formulated in the half-range of the singular variable.

The general solution to the RTE in the half-space $z > 0$ can be written as a superposition of outgoing evanescent waves of the form (44):

$$I(\mathbf{r}, \hat{\mathbf{s}}) = \int \frac{d^2q}{(2\pi)^2} \sum_{\mu}' F_{\mathbf{q},\mu}^{(+)} I_{\mathbf{q},\mu}^{(+)}(\mathbf{r}, \hat{\mathbf{s}}) , \quad (48)$$

where the unknown coefficients $F_{\mathbf{q},\mu}^{(+)}$ must be found from the boundary condition (47). Now we use expansion (48) and expression (44) to calculate $I_0(\boldsymbol{\rho}, \hat{\mathbf{s}})$. Upon Fourier transformation of (47) with respect to $\boldsymbol{\rho}$, we arrive at the following equation:

$$\sum_{lm} \sum_{\mu}' Y_{lm}(\hat{\mathbf{s}}; \hat{\mathbf{z}}) \langle lm | \mathcal{A}(\hat{\mathbf{q}}) | \eta_{\mu}(q) \rangle F_{\mathbf{q},\mu}^{(+)} = I_{\text{inc}}(\mathbf{q}, \hat{\mathbf{s}}) , \quad \text{if } \hat{\mathbf{s}} \cdot \hat{\mathbf{z}} > 0 . \quad (49)$$

Next, we multiply both sides of Eq. 49 by $Y_{l'm'}^*(\hat{\mathbf{s}}; \hat{\mathbf{z}})$ and integrate over all directions such that $\hat{\mathbf{s}} \cdot \hat{\mathbf{z}} > 0$. Note that integration in the right-hand side can be extended to all directions of $\hat{\mathbf{s}}$ since $I_{\text{inc}}(\mathbf{q}, \hat{\mathbf{s}})$ is identically zero for $\hat{\mathbf{s}} \cdot \hat{\mathbf{z}} < 0$. Thus, for a collimated narrow incident beam which crosses the boundary at $\boldsymbol{\rho} = \boldsymbol{\rho}_0$ in the direction $\hat{\mathbf{s}}_0$, we obtain

$$\sum_{\mu}' \langle lm | \mathcal{B} \mathcal{A}(\hat{\mathbf{q}}) | \eta_{\mu}(q) \rangle F_{\mathbf{q},\mu}^{(+)} = \exp(-i\mathbf{q} \cdot \boldsymbol{\rho}_0) Y_{lm}^*(\hat{\mathbf{s}}_0; \hat{\mathbf{z}}) , \quad (50)$$

where matrix \mathcal{B} is given by

$$\begin{aligned} \langle lm | \mathcal{B} | l'm' \rangle &= \int_{\hat{\mathbf{s}} \cdot \hat{\mathbf{z}} > 0} Y_{lm}^*(\hat{\mathbf{s}}; \hat{\mathbf{z}}) Y_{l'm'}(\hat{\mathbf{s}}; \hat{\mathbf{z}}) d^2s \\ &= \frac{\delta_{mm'}}{2} \sqrt{\frac{(2l+1)(2l'+1)(l-m)!(l'-m)!}{(l+m)!(l'+m)!}} \int_0^1 P_l^m(x) P_{l'}^m(x) dx . \end{aligned} \quad (51)$$

For a fixed value of \mathbf{q} , (50) is a set of linear equations of infinite size. In practice, this set must be truncated so that $l < l_{\text{max}}$. Then the number of equations is $2N = (l_{\text{max}}+1)^2$, where we have assumed for simplicity that l_{max} is odd. But the number of unknowns $F_{\mathbf{q},\mu}^{(+)}$ is only equal to N , since $\mu \in \Omega^+$. Therefore, (50) is formally overdetermined. However, not all equations in (50) are linearly independent. In fact, the rank of \mathcal{B} is

exactly equal to half of its size, which is a consequence of half-range integration in (51). Therefore we come to the conclusion that (50) is a well-determined system of equations with respect to N unknowns $F_{\mathbf{q},\mu}^{(+)}$.

Numerically, the problem can be solved in two different ways. A direct approach is to consider only equations in (50) which are linearly independent. This is achieved by only leaving equations in the system with l having the same parity as m , e.g., for a fixed m , $l = |m|, |m| + 2, |m| + 4, \dots$, with the restriction $l \leq l_{\max}$. Another approach is to seek the generalized Moore-Penrose pseudoinverse of (50). In this case eigenvectors of the truncated matrix \mathcal{B} must be found numerically. If the size of \mathcal{B} is even, half of its eigenvalues will be zero. Let $|\xi_\nu\rangle$ be the eigenvectors of \mathcal{B} with nonzero eigenvalues α_ν . Then the system of equations (50) can be rewritten as

$$\alpha_\nu \sum_\mu' \langle \xi_\nu | \mathcal{A}(\hat{\mathbf{q}}) | \eta_\mu(q) \rangle F_{\mathbf{q},\mu}^{(+)} = \exp(-i\mathbf{q} \cdot \boldsymbol{\rho}_0) \sum_{lm} \langle \xi_\nu | lm \rangle Y_{lm}^*(\hat{\mathbf{s}}_0; \hat{\mathbf{z}}) . \quad (52)$$

We note that in the limit $l_{\max} \rightarrow \infty$, the eigenvectors of \mathcal{B} are known and are of simple form: $\langle lm | \xi_{\hat{\mathbf{s}}} \rangle = Y_{lm}^*(\hat{\mathbf{s}}; \hat{\mathbf{z}})$ with the eigenvalues being unity for $\hat{\mathbf{s}} \cdot \hat{\mathbf{z}} > 0$ and zero otherwise, i.e., \mathcal{B} is idempotent.

The system (52) can be simplified by the substitution $F_{\mathbf{q},\mu}^{(+)} = f_{\mathbf{q},\mu}^{(+)} \exp(-i\mathbf{q} \cdot \boldsymbol{\rho}_0)$. The coefficients $f_{\mathbf{q},\mu}^{(+)}$ are then independent of the source coordinate $\boldsymbol{\rho}_0$. Another simplification is achieved by noting that both \mathcal{A} and \mathcal{B} are diagonal in indices m and m' . Effectively, system (52) must be solved once for each value of the *absolute value* q ; dependence of the solution on the direction of \mathbf{q} is trivial. If, in addition, the incident beam is normal to the interface ($\hat{\mathbf{s}}_0 = \hat{\mathbf{z}}$), the solutions do not depend on $\hat{\mathbf{q}}$ at all.

The additional computational complexity associated with solving the boundary value problem is then as follows. For every numerical value of the lengths of the vector \mathbf{q} which is used in the expansion (48), a system of linear equations of the size $N = (l_{\max} + 1)^2$ must be solved (complexity of diagonalization of \mathcal{B} is negligibly small). Thus, consideration of boundary conditions adds significant computational complexity to the problem. This is the consequence of the fact that the rotation matrices $\exp[\tau(q\lambda_\mu)J_y]$, unlike the matrix W , are not diagonal in m and m' . As a result, the system of equations (52) is not block diagonal and, in addition, q -dependent. However, the problem is easily solvable on modern computers for $l_{\max} \leq 100$, which is, perhaps, more than is needed in any practical computation.

3.6.2. External source incident on a slab

Generalization of the mathematical apparatus developed in Section 3.6.1 to the case of RTE in a finite slab is straightforward. Consider RTE in a slab $0 < z < L$. The external source is assumed to be incident from the left. Then the boundary conditions read

$$I_0(\boldsymbol{\rho}, \hat{\mathbf{s}}) = I_{\text{inc}}(\boldsymbol{\rho}, \hat{\mathbf{s}}) , \quad \text{if } \hat{\mathbf{s}} \cdot \hat{\mathbf{z}} > 0 , \quad (53)$$

$$I_L(\boldsymbol{\rho}, \hat{\mathbf{s}}) = 0 , \quad \text{if } \hat{\mathbf{s}} \cdot \hat{\mathbf{z}} < 0 , \quad (54)$$

where I_0 and I_L are the specific intensities evaluated at the surfaces $z = 0$ and $z = L$, respectively. The general solution inside the slab has the form

$$I(\mathbf{r}, \hat{\mathbf{s}}) = \int \frac{d^2q}{(2\pi)^2} \sum_{\mu}' \left[F_{\mathbf{q},\mu}^{(+)} I_{\mathbf{q},\mu}^{(+)}(\mathbf{r}, \hat{\mathbf{s}}) + F_{-\mathbf{q},\mu}^{(-)} I_{-\mathbf{q},\mu}^{(-)}(\mathbf{r}, -\hat{\mathbf{s}}) \right] , \quad (55)$$

where $F_{\mathbf{q},\mu}^{(+)}$ and $F_{\mathbf{q},\mu}^{(-)}$ are unknown coefficients. After some manipulations, we arrive at the following system of equations:

$$\sum_{\mu}' \left\{ \langle lm | \mathcal{BA}(\hat{\mathbf{q}}) | \eta_{\mu}(q) \rangle F_{\mathbf{q},\mu}^{(+)} + \exp[-Q_{\mu}(q)L] \langle l, -m | \mathcal{BA}^{\dagger}(\hat{\mathbf{q}}) | \eta_{\mu}(q) \rangle F_{\mathbf{q},\mu}^{(-)} \right\} = \exp(-i\mathbf{q} \cdot \boldsymbol{\rho}_0) Y_{lm}^*(\hat{\mathbf{s}}_0; \hat{\mathbf{z}}) , \quad (56)$$

$$\sum_{\mu}' \left\{ \exp[-Q_{\mu}(q)L] \langle lm | \mathcal{BA}(\hat{\mathbf{q}}) | \tilde{\eta}_{\mu}(q) \rangle F_{\mathbf{q},\mu}^{(+)} + \langle l, -m | \mathcal{BA}^{\dagger}(\hat{\mathbf{q}}) | \tilde{\eta}_{\mu}(q) \rangle F_{\mathbf{q},\mu}^{(-)} \right\} = 0 . \quad (57)$$

This set of equations is an analog of (50) for the case of a finite slab. In the limit $L \rightarrow \infty$ one has $F_{\mathbf{q},\mu}^{(-)} = 0$ and (56) coincides with (50). We note that for a fixed \mathbf{q} , (56),(57) is a set of $2N$ linearly independent equations for $2N$ unknowns. The methods of linear algebra briefly discussed in Section 3.6.1 can be used to obtain solution.

3.6.3. Internal source in a half-space

Next, we consider an internal source in the half-space $z > 0$. Here we assume that there are no external sources. However, if this is not so, the solution can be obtained by simple superposition.

Consider a point unidirectional source of the form $\varepsilon = \delta(\boldsymbol{\rho} - \boldsymbol{\rho}_0) \delta(z - z_0) \delta(\hat{\mathbf{s}} - \hat{\mathbf{s}}_0)$, where $z_0 > 0$. The general solution in the region $z > 0$ is written as

$$I(\mathbf{r}, \hat{\mathbf{s}}) = \int \frac{d^2q}{(2\pi)^2} \sum_{\mu}' \left[V_{\mathbf{q},\mu} I_{-\mathbf{q},\mu}^{(-)}(\mathbf{r}_0, -\hat{\mathbf{s}}_0) + F_{\mathbf{q},\mu}^{(+)} \right] I_{\mathbf{q},\mu}^{(+)}(\mathbf{r}, \hat{\mathbf{s}}) , \quad (58)$$

The boundary condition at the interface $z = 0$ is homogeneous:

$$I_0(\boldsymbol{\rho}, \hat{\mathbf{s}}) = 0 , \quad \text{if } \hat{\mathbf{s}} \cdot \hat{\mathbf{z}} > 0 . \quad (59)$$

By analogy with Section 3.6.1, we immediately arrive at the following set of equations for the unknown coefficients $F_{\mathbf{q},\mu}^{(+)}$:

$$\sum_{\mu}' \langle lm | \mathcal{BA}(\hat{\mathbf{q}}) | \eta_{\mu}(q) \rangle \left[F_{\mathbf{q},\mu}^{(+)} + V_{\mathbf{q},\mu} I_{-\mathbf{q},\mu}^{(-)}(\mathbf{r}_0, -\hat{\mathbf{s}}_0) \right] = 0 . \quad (60)$$

Similarly to (50), this is a set of N linearly independent equations with respect to N unknowns.

4. Numerics

Now we illustrate expressions obtained in Section 3.3 for the RTE Green's function in an infinite medium with several numerical examples. We have computed the Green's function by truncating the series in (23) at $l, l' \leq l_{\max}$ and using the reference frame in which the z -axis is aligned with the direction of the source, $\hat{\mathbf{s}}_0$. Correspondingly, expression (26) was used to compute the matrix elements of χ . Note that in this expression the summation over M and j is finite; however, summation over the modes $|\psi_\mu\rangle$ is infinite and must be truncated. We have found empirically that summation over $N = 500$ eigenmodes (which corresponds to $1,000 \times 1,000$ matrices W) is sufficient for all cases shown below. Further increase of N does not change the result within the double precision machine accuracy. The results start to deviate noticeably from those computed at $N = 500$ when N is taken to be smaller than ~ 100 , especially when l_{\max} is relatively large. Further, we have used the Henyey-Greenstein model for the phase function, so that $A_l = g^l$ where $0 < g < 1$ is a parameter. In all figures shown below we calculate the specific intensity $I(\mathbf{r}, \hat{\mathbf{s}})$ due to a point unidirectional source placed at the origin and illuminating in the z -direction. The distance from the source is measured in units of the transport free path, $\ell^* = 1/[\mu_a + (1 - g)\mu_s]$, which plays an important role in diffusion theory.

It should be noted that numerical implementation of the formulas derived in this paper requires a degree of caution because the Green's function of the RTE is not square integrable with respect to both of its arguments, \mathbf{r} and $\hat{\mathbf{s}}$. Therefore, one can not expect uniform point-wise conversion of the result with l_{\max} . Mathematically, this is manifested in the fact that the Bessel functions $k_l(x)$ that enter into (25),(26) diverge factorially for large orders: $k_l(x) \propto l!!$ ($l \rightarrow \infty$). This growth can be compensated neither by the Clebsch-Gordan coefficients, nor by the eigenvector components $\langle lm|\psi_\mu\rangle$ which decay, at best, exponentially (see discussion in Section 3.2.3). Therefore, (23),(25),(26) must be viewed as expressions defining the *moments* of the Green's function and the latter as a generalized function or a distribution. Nevertheless, in most practical situations, the spatial and angular dependencies of the Green's function can be approximated by smooth square-integrable functions by truncating (23) at certain values of l_{\max} that provide desirable angular resolution. Computations are further facilitated by analytical subtraction of the *ballistic component* of the Green's function:

$$G_b(\mathbf{r}, \hat{\mathbf{s}}; \mathbf{r}_0, \hat{\mathbf{s}}_0) = \delta(\hat{\mathbf{s}} - \hat{\mathbf{s}}_0)\delta(\hat{\mathbf{R}} - \hat{\mathbf{s}}_0)\frac{\exp(-\mu_t R)}{R^2}, \quad \mathbf{R} = \mathbf{r} - \mathbf{r}_0. \quad (61)$$

The corresponding ballistic contribution to χ_b is

$$\langle lm|\chi_b(R; \hat{\mathbf{s}}_0)|l'm'\rangle = \delta_{m0}\sqrt{(2l+1)(2l'+1)}\frac{\exp(-\mu_t R)}{4\pi R^2}, \quad (62)$$

However, it is impossible to remove the singularities *completely*, and the remainder of such subtraction still remains non-square integrable.

The effect of subtraction of the ballistic term and convergence with l_{\max} for the forward propagation is illustrated in Fig. 2. Here θ is the angle between the direction

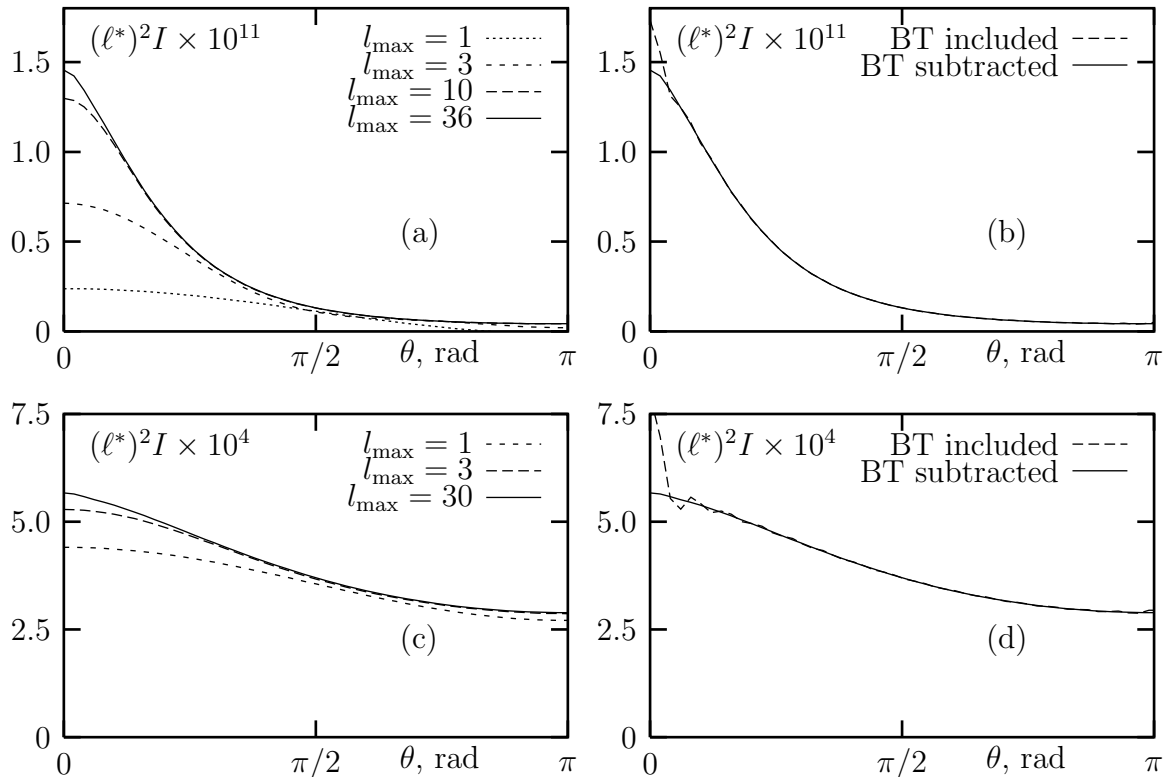


Figure 2. Angular dependence of the specific intensity for forward propagation at the distance z from the source. Left column (a,c): convergence with parameter l_{\max} . Right column (b,d): solid line shows the converged result obtained with subtraction of the ballistic term; dashed line: result obtained without subtraction of the ballistic term for the same l_{\max} . Top row (a,b): $g = 0.5$, $\mu_a/\mu_s = 0.5$, $z = 20\ell^*$. Bottom row (c,d): $g = 0.2$, $\mu_a/\mu_s = 0.01$ and $z = 10\ell^*$.

of observation, $\hat{\mathbf{s}}$, and the positive direction of the z -axis: $\cos\theta = \hat{\mathbf{s}} \cdot \hat{\mathbf{z}}$. In the left column (plots a,c) we show the dependence of the specific intensity (with the ballistic term subtracted) on the maximum order of spherical functions l_{\max} . We assumed that convergence was reached when incrementing l_{\max} by 1 resulted in less than 0.1% relative change of the specific intensity in any direction. However, we emphasize again that this convergence is asymptotic. In the right column of images (b,d), we compare the angular dependence of the specific intensity for the maximum value of l_{\max} which was used in the graph to the left with and without the ballistic term. Note that the subtracted ballistic term can be added back analytically to the obtained solutions. In all figures below, the ballistic term is subtracted.

Fig. 3 illustrates the specific intensity for the forward and backward propagation. Optical parameters are chosen to be close to those of typical biological tissues in the near infrared spectral region (see figure caption for details). The point of observation is placed at $\mathbf{r} = (0, 0, z)$, where z is positive for forward propagation and negative for backward propagation, and θ is defined in both cases as the angle between the vector $\hat{\mathbf{s}}$ and the positive direction of the z -axis. It can be seen from the figure that the

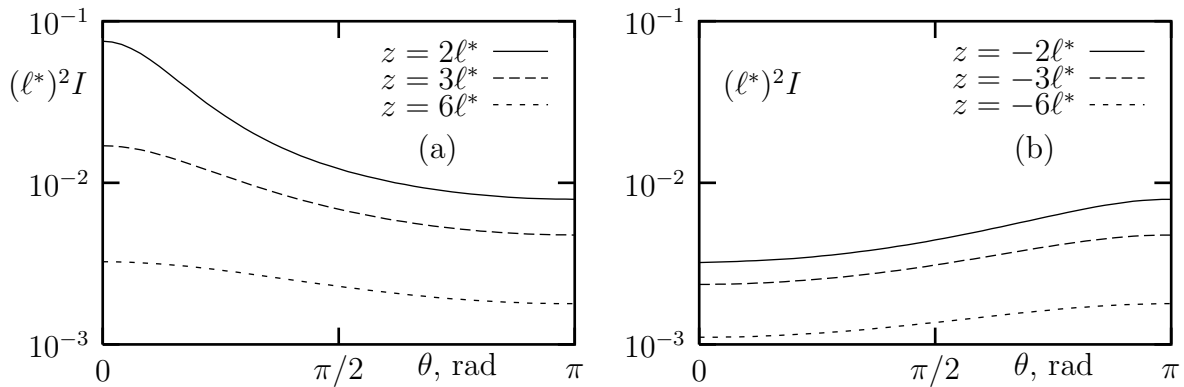


Figure 3. Angular dependence of the specific intensity for forward (a) and backward (b) propagation obtained at $l_{\max} = 21$, $g = 0.98$ and $\mu_a/\mu_s = 6 \cdot 10^{-5}$. The distance to the source z is assumed to be positive for forward propagation and negative for backward propagation.

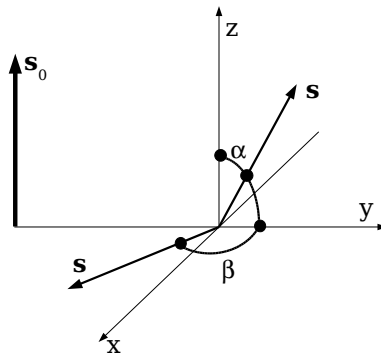


Figure 4. Illustration of angles α and β .

specific intensity in the backward direction is significantly smaller compared to that in the forward direction, even at relatively large source-detector separations ($|z| = 6\ell^*$). It can be also seen that the angular distribution of the specific intensity in the forward direction is more sharply peaked than that in the backward direction. This can be explained by noticing that backward propagation involves more scattering events than same distance forward propagation.

Now we turn to the off-axis case. Here the source is still placed at the origin and illuminates in the positive z direction, while the point of observation is placed at a point $\mathbf{r} = (0, y, 0)$. Below, we show two type of graphs. In the first case the vector $\hat{\mathbf{s}}$ is in the $y - z$ plane, and its orientation is characterized by the angle α with respect to the positive direction of z -axis. In the second case, $\hat{\mathbf{s}}$ is in the $x - y$ plane (perpendicular to $\hat{\mathbf{s}}_0$) and is characterized by the angle β with respect to the positive direction of the y -axis. The angles α and β (not to be confused with the Euler angles) are illustrated in Fig. 4. Note that α varies from 0 to 2π while β is restricted to the interval $[0, \pi]$ due to the obvious symmetry.

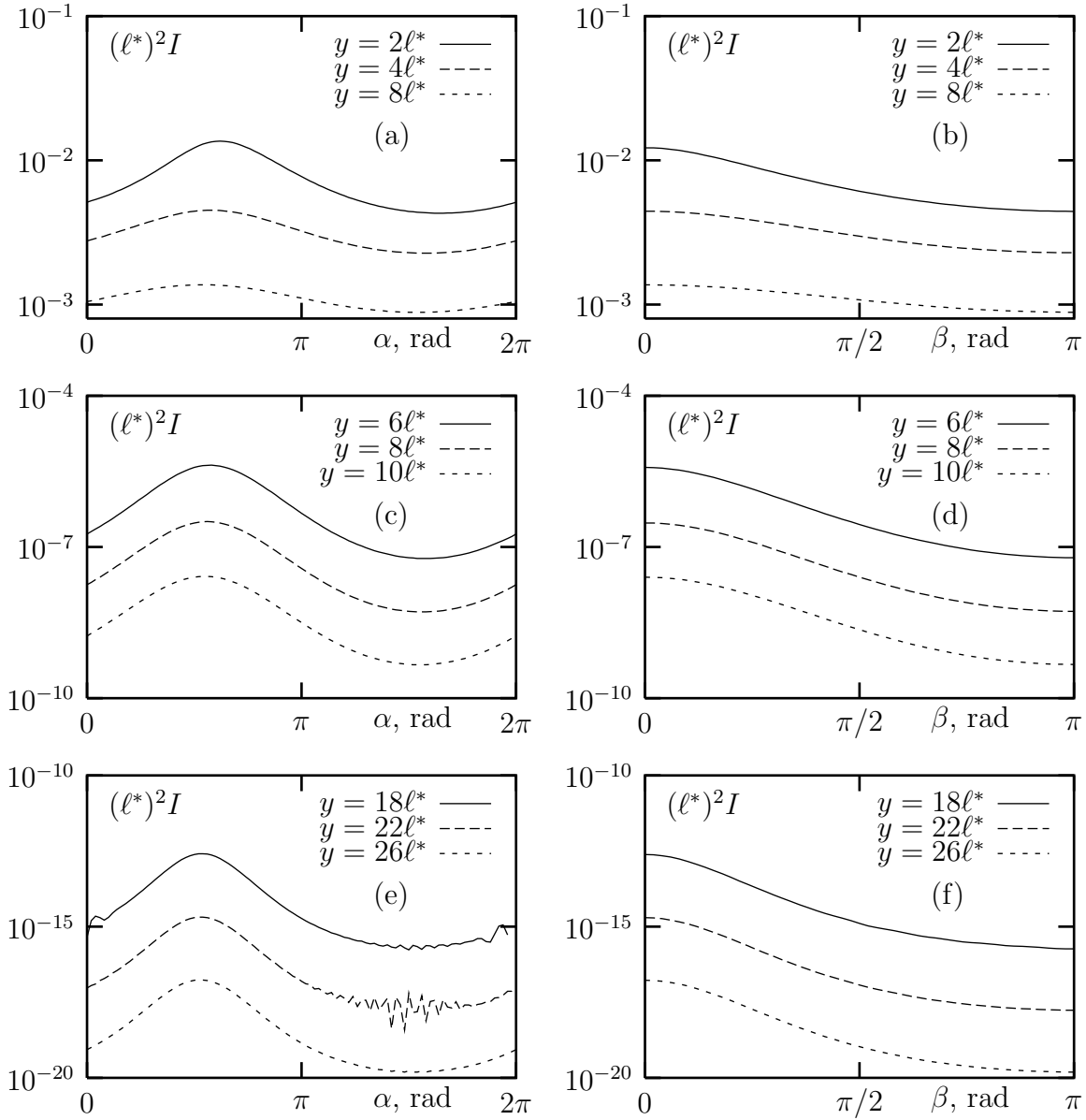


Figure 5. Angular distribution of specific intensity for off-axis propagation. Parameters: $g = 0.98$ and $\mu_a/\mu_s = 6 \cdot 10^{-5}$ (a,b), $\mu_a/\mu_s = 0.03$ (c,d), $\mu_a/\mu_s = 0.2$ (e,f).

In Fig. 5 we illustrate the specific intensity for highly forward-peaked scattering ($g = 0.98$) and the following three different ratios of μ_a/μ_s : $6 \cdot 10^{-5}$, 0.03 and 0.2. Note that the corresponding ratios of μ_a/μ'_s , where $\mu'_s = (1 - g)\mu_s$ is the reduced scattering coefficient, are 0.003, 1.5 and 10, respectively. In the first case the transport free path is mainly determined by scattering, while in the third case it is determined by absorption. The left column of images (a,c,e) illustrate the angular dependence of the specific intensity as a function of the angle α (vector $\hat{\mathbf{s}}$ is in the $y - z$ plane). The noise visible in Fig. 5(e) is due to the non-square integrability discussed above. However, the

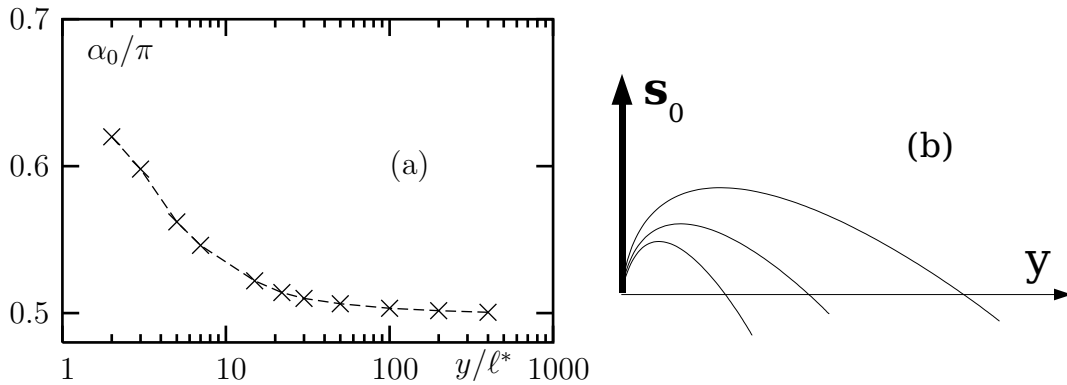


Figure 6. (a) Dependence of the position of maximum α_0 on the distance to the source, y , for physiological parameters: $g = 0.98$ and $\mu_a/\mu_s = 6 \cdot 10^{-5}$. (b) Schematic illustration of typical “photon trajectories” that correspond to maxima in graphs 5(a,c,e).

values of the specific intensity at the region where the noise is visible are two to three orders of magnitude smaller than those at the peak.

It is interesting analyze the position of the maximum of the curves in Fig. 5(a,c,e), α_0 . As the distance between the source and the detector increases, α_0 approaches $\pi/2$. This corresponds to a vector $\hat{\mathbf{s}}$ coinciding with the direction from the source to detector. However, for relatively small source-detector separations, α_0 is larger than $\pi/2$. The dependence of α_0 on the source-detector separation is illustrated in Fig. 6(a) for physiological parameters. The dependence of α_0 on the source-detector separation can be understood at the qualitative level. Indeed, at large separations, the angular distribution of the specific intensity is expected to be independent of the source orientation, with the maximum attained when $\hat{\mathbf{s}}$ is aligned with the direction from the source to the detector. This corresponds to $\alpha_0 = \pi/2$. At smaller separations, the “photons” arrive at the detector locations along some “typical” (most probable) trajectories which are schematically illustrated in Fig. 6(b). We assume here that α_0 is determined by the angle at which the most probable trajectory crosses the y -axis.

In Fig. 5(b,d,f), the specific intensity is shown as a function of the angle β (vector $\hat{\mathbf{s}}$ is in the $x - y$ plane). In this case the maximum of the curves always corresponds to $\beta = 0$, which could be also inferred from the symmetry. We note that $I_{xy}(\beta = 0) = I_{yz}(\alpha = \pi/2)$, where the lower subscripts indicate the plane in which contains the vector $\hat{\mathbf{s}}$.

The curves shown in Fig. 5 have the dynamic range of approximately 10^3 . The dynamic range of this magnitude was obtained due to the use of large values of l_{\max} . For smaller values of l_{\max} , the result can be grossly inaccurate and even negative. For example, in Fig. 7 we illustrate convergence with l_{\max} to one of the curves shown in Fig. 5(e). An accurate value of specific intensity at $\alpha \approx \pi/2$ ($\approx 10^{-3}$ relative error) was obtained at $l_{\max} = 39$. Note that at $l_{\max} = 10$, the computed specific intensity is still grossly inaccurate.

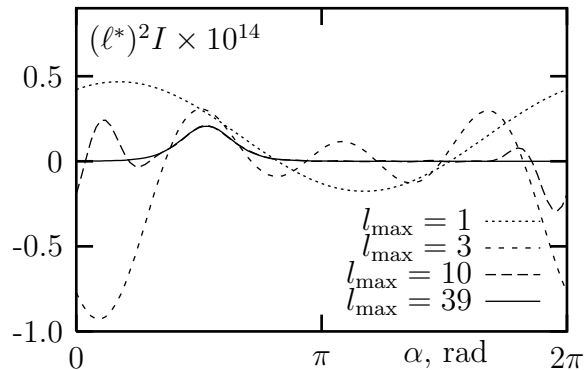


Figure 7. Convergence of the specific intensity with l_{\max} for $g = 0.98$, $\mu_a/\mu_s = 0.2$ and $y = 22\ell^*$.

5. Discussion

The theoretical approach developed in this paper is, essentially, a spectral approach. The spectral methods have been studied extensively for the one-dimensional RTE [25]. However, in the 3D case these methods become very difficult to use. The substantially novel element of this paper is that we derive a practically usable spectral method for the full three-dimensional RTE with an arbitrary phase function and planar boundaries. The analytical part of obtained solution is of considerable complexity. However, this complexity is traded for the relative simplicity of the numerical part. In fact, we believe that we have reduced the numerical part of the computations to the absolute minimum which is allowed by the mathematical nature of the problem.

Consideration in this paper is limited to spatially-independent optical coefficients and phase function. However, we note that the Green's function for macroscopically homogeneous medium is of special interest, since it is used in linearized image reconstruction in optical tomography [26] and, more generally, in nonlinear image reconstruction based on inversion of functional series or the Newton-Kantorovich method [27]. The linearized kernel of the integral equation of diffusion tomography has the form (in the slab imaging geometry) [26]

$$\Gamma(\boldsymbol{\rho}_1, \boldsymbol{\rho}_2; \mathbf{r}) = \int G(\boldsymbol{\rho}_1, z = 0, \hat{\mathbf{s}}_1 = \hat{\mathbf{z}}; \mathbf{r}, \hat{\mathbf{s}}) G(\mathbf{r}, \hat{\mathbf{s}}; \boldsymbol{\rho}_2, z = L, \hat{\mathbf{s}}_2 = \hat{\mathbf{z}}) d^2 s, \quad (63)$$

where G is the Green's function in a slab with constant absorption and scattering coefficients. One of the advantages of solutions obtained in this paper, compared to those based on discrete ordinates, is that the angular integral in the above formula can be evaluated analytically.

Appendix A. Calculation of integral (24)

In this Appendix we evaluate integral (24) for different choices of $\hat{\mathbf{z}}$. Written in components, this integral reads

$$\begin{aligned}
\langle lm|\chi(\mathbf{r};\hat{\mathbf{z}})|l'm'\rangle &= \frac{1}{\sqrt{\sigma_l\sigma_{l'}}} \sum_{m_1=-l}^l \sum_{m_2=-l'}^{l'} \\
&\times \int \frac{d^3\mathbf{k}}{(2\pi)^3} \exp(i\mathbf{k}\cdot\mathbf{r}) \exp[-i(m-m')\varphi_{\hat{\mathbf{k}}}] \\
&\times d_{mm_1}^l(\theta_{\hat{\mathbf{k}}}) d_{m'm_2}^{l'}(\theta_{\hat{\mathbf{k}}}) \sum_{\mu} \frac{\langle lm_1|\psi_{\mu}\rangle\langle\psi_{\mu}|l'm_2\rangle}{1+ik\lambda_{\mu}}. \quad (\text{A.1})
\end{aligned}$$

We start with the case $\hat{\mathbf{z}} = \hat{\mathbf{r}}$. Then we have $\mathbf{k}\cdot\hat{\mathbf{r}} = kr \cos\theta_{\hat{\mathbf{k}}}$. We also notice that $\langle lm_1|\psi_{\mu}\rangle\langle\psi_{\mu}|l'm_2\rangle \propto \delta_{m_1m_2}$, so that the summation over m_1 and m_2 can be replaced by summation over a single index M which runs from $-\bar{l}$ to \bar{l} , where $\bar{l} = \min(l, l')$. Then (A.1) can be rewritten as

$$\langle lm|\chi(\mathbf{r};\hat{\mathbf{r}})|l'm'\rangle = \frac{1}{\sqrt{\sigma_l\sigma_{l'}}} \sum_{M=-\bar{l}}^{\bar{l}} \int_0^{\infty} \frac{k^2 dk}{(2\pi)^2} \sum_{\mu} \frac{\langle lM|\psi_{\mu}\rangle\langle\psi_{\mu}|l'M\rangle}{1+ik\lambda_{\mu}} \times I, \quad (\text{A.2})$$

where I is the angular part of the integral (the list of formal arguments of I is omitted):

$$I = \int \frac{\sin\theta_{\hat{\mathbf{k}}} d\theta_{\hat{\mathbf{k}}} d\varphi_{\hat{\mathbf{k}}}}{2\pi} \exp[i(m'-m)\varphi_{\hat{\mathbf{k}}}] \exp(ikr \cos\theta_{\hat{\mathbf{k}}}) d_{mM}^l(\theta_{\hat{\mathbf{k}}}) d_{m'M}^{l'}(\theta_{\hat{\mathbf{k}}}). \quad (\text{A.3})$$

Integral over $\varphi_{\hat{\mathbf{k}}}$ is evaluated immediately with the result of $2\pi\delta_{mm'}$. Integration over $\theta_{\hat{\mathbf{k}}}$ requires expanding the exponent in the integrand as

$$\exp(ikr \cos\theta_{\hat{\mathbf{k}}}) = \sum_{L=0}^{\infty} i^L (2L+1) j_L(kr) d_{00}^L(\theta_{\hat{\mathbf{k}}}), \quad (\text{A.4})$$

where $j_l(x)$ are the spherical Bessel functions of the first kind, and using the following formula (see Ref. [24], Sect. 4.11.2, formula 8, and the symmetry properties of d-functions given in Sect. 4.11, formula 1 of the same reference):

$$\int_0^{\pi} d_{mM}^l(\theta) d_{m'M}^{l'}(\theta) d_{00}^L(\theta) \sin\theta d\theta = \frac{2(-1)^{m-M}}{2L+1} C_{l,m,l',-m}^{L,0} C_{l,M,l',-M}^{L,0}, \quad (\text{A.5})$$

where $C_{j_1 m_1 j_2 m_2}^{j_3 m_3}$ are the Clebsch-Gordan coefficients. Taking into account that $C_{l,m,l',-m}^{L,0}$ is nonzero only for $|l-l'| \leq L \leq l+l'$, we obtain

$$I = 2\delta_{mm'} (-1)^{m-M} \sum_{L=|l-l'|}^{l+l'} i^L j_L(kr) C_{l,m,l',-m}^{L,0} C_{l,M,l',-M}^{L,0}. \quad (\text{A.6})$$

Next, we substitute this result into (A.5) and, after some rearrangement, arrive at

$$\begin{aligned}
\langle lm|\chi(\mathbf{r};\hat{\mathbf{r}})|l'm'\rangle &= \frac{2\delta_{mm'} (-1)^m}{\sqrt{\sigma_l\sigma_{l'}}} \sum_{M=-\bar{l}}^{\bar{l}} (-1)^M \sum_{L=|l-l'|}^{l+l'} i^L C_{l,m,l',-m}^{L,0} C_{l,M,l',-M}^{L,0} \\
&\times \sum_{\mu} \langle lM|\psi_{\mu}\rangle\langle\psi_{\mu}|l'M\rangle \int_0^{\infty} \frac{k^2 dk}{(2\pi)^2} \frac{j_L(kr)}{1+ik\lambda_{\mu}}. \quad (\text{A.7})
\end{aligned}$$

To evaluate the radial integral, we exploit the symmetry properties of the above expression. First, we notice that $C_{l,M,l',-M}^{L,0} = (-1)^{l+l'+L} C_{l,-M,l',M}^{L,0}$, while $\langle lM|\psi_\mu\rangle$ do not depend on the sign of M . Thus, addition of terms with positive and negative values of M in the above formula (for $M \neq 0$) gives zero unless $l+l'+L$ is even. Likewise, in the case $M = 0$, $C_{l,0,l',0}^{L,0} = 0$ unless the above sum of indices is even. Correspondingly, the only nonzero contributions to the sum over L correspond to $L = |l-l'| + 2j$, where the index j runs from 0 to \bar{l} . Next, we use the symmetry property of the eigenvectors discussed in Section 3.2.2. This property allows one to limit summation over the eigenvector indices μ to only the values corresponding to positive eigenvalues λ_μ while simultaneously replacing the factor $1/(1+ik\lambda_\mu)$ by $1/(1+ik\lambda_\mu) + (-1)^{l+l'}/(1-ik\lambda_\mu)$. Thus, we obtain

$$\begin{aligned} \langle lm|\chi(\mathbf{r}; \hat{\mathbf{r}})|l'm'\rangle &= \frac{2\delta_{mm'}(-1)^m}{\sqrt{\sigma_l\sigma_{l'}}} \sum_{M=-\bar{l}}^{\bar{l}} (-1)^M \sum_{j=0}^{\bar{l}} i^{|l-l'|+2j} C_{l,m,l',-m}^{|l-l'|+2j,0} C_{l,M,l',-M}^{|l-l'|+2j,0} \\ &\quad \times \sum_{\mu} \langle lM|\psi_\mu\rangle \langle \psi_\mu|l'M\rangle \times J, \end{aligned} \quad (\text{A.8})$$

where J is the radial integral given by

$$J = \int_0^\infty \frac{k^2 dk}{(2\pi)^2} j_{|l-l'|+2j}(kr) \frac{1 + (-1)^{l+l'} - ik\lambda_\mu [1 - (-1)^{l+l'}]}{1 + k^2\lambda_\mu^2}. \quad (\text{A.9})$$

The parity of Bessel functions in the above integral is the same as that of $l+l'$. Therefore, the integrand is an even function of k for all values of indices, and the integral can be extended to $-\infty$ and calculated by residues. The result is

$$J = \pi i^{-(l-l'+2j)} \lambda_\mu^{-3} k_{|l-l'|+2j}(r/\lambda_\mu). \quad (\text{A.10})$$

Upon substitution of this result into (A.8), we obtain formula (25).

In the case $\hat{\mathbf{z}} = \hat{\mathbf{s}}_0$ the dot product $\mathbf{k} \cdot \mathbf{r}$ can not be written as $kr \cos\theta_{\hat{\mathbf{k}}}$. Therefore, the exponent in the angular integral I is expanded as

$$\exp(i\mathbf{k} \cdot \mathbf{r}) = 4\pi \sum_{LM'} i^L j_L(kr) Y_{LM'}(\hat{\mathbf{k}}; \hat{\mathbf{s}}_0) Y_{LM'}^*(\hat{\mathbf{r}}; \hat{\mathbf{s}}_0). \quad (\text{A.11})$$

We further take advantage of the identity

$$Y_{LM'}(\theta_{\hat{\mathbf{k}}}, \varphi_{\hat{\mathbf{k}}}) = (-1)^{M'} \sqrt{4\pi/(2L+1)} d_{0M'}^L(\theta_{\hat{\mathbf{k}}}) \exp(iM'\varphi_{\hat{\mathbf{k}}}) \quad (\text{A.12})$$

to transform the angular integration to the general form (A.6). Note that azimuthal integration results in a factor of $\delta_{M'm}$ and thus removes summation over M' . The final result for I is

$$I = 2(-1)^M \sum_{L=|l-l'|}^{l+l'} \sqrt{\frac{4\pi}{2L+1}} i^L j_L(kr) Y_{Lm}^*(\hat{\mathbf{r}}; \hat{\mathbf{s}}_0) C_{l,M,l',-M}^{L,0} C_{l,m,l',0}^{L,m}. \quad (\text{A.13})$$

The radial integration, and the symmetry considerations explained above, remain without change. Substitution of (A.13) into (A.2) and subsequent radial integration leads to the formula (26).

Appendix B. Calculation of integral (28)

Integral (28), written in components, reads

$$\langle lm|\kappa(\mathbf{q}; z)|l'm'\rangle = \frac{\exp[-i(m-m')]}{\sqrt{\sigma_l\sigma_{l'}}} \sum_{M=-\bar{l}}^{\bar{l}} \sum'_n \frac{\langle l|\phi_n(M)\rangle\langle\phi_n(M)|l'\rangle}{\lambda_{nM}^2} \times I, \quad (\text{B.1})$$

where I is the integral over k_z :

$$I = \int_{-\infty}^{\infty} \frac{dk_z}{2\pi} \exp(ik_z z) d_{mM}^l(\theta) d_{m'M}^{l'}(\theta) \frac{1 + (-1)^{l+l'} - i\lambda_{Mn}\sqrt{q^2 + k_z^2}[1 - (-1)^{l+l'}]}{k_z^2 + q^2 + 1/\lambda_{Mn}^2}, \quad (\text{B.2})$$

where we have used the notations introduced in Section 3.2.1 for block eigenvectors $|\phi_n(M)\rangle$. The angle θ is defined by (29) in Section 3.4. The Wigner d-functions can be written in terms of $\cos\theta$ as

$$d_{mM}^l(\theta) = \xi_{mM} Z_{mM}^l \left(\frac{1 - \cos\theta}{2}\right)^{\frac{|m-M|}{2}} \left(\frac{1 + \cos\theta}{2}\right)^{\frac{|m+M|}{2}} P_s^{(u,v)}(\cos\theta), \quad (\text{B.3})$$

where $\xi_{mM} = 1$ if $m \leq M$ and $\xi = (-1)^{m+M}$ if $m > M$,

$$Z_{mM}^l = \sqrt{\frac{(l - |m - M|/2 - |m + M|/2)! (l + |m + M|/2 - |m + M|/2)!}{(l + |m - M|/2 - |m + M|/2)! (l - |m + M|/2 - |m + M|/2)!}}, \quad (\text{B.4})$$

and $P_s^{(u,v)}(x)$ in expression (B.3) are Jacobi polynomials with $s = l - |m - M|/2 - |m + M|/2$, $u = |m - M|$ and $v = |m + M|$.

The integrand in (B.2) is not, in general, an analytical function of k_z . However, the expression for the Green's function contains summation over M . It can be shown explicitly that the combination

$$d_{mM}^l(\theta) d_{m'M}^{l'}(\theta) + d_{m-M}^l(\theta) d_{m'-M}^{l'}(\theta) \quad (\text{B.5})$$

contains only even powers of the factor $\sqrt{k_z^2 + q^2}$ if $l + l'$ is even and only odd powers of the same factor if $l + l'$ is odd (a general proof of this statement is available but omitted). Taking into account the factor $\sqrt{q^2 + k_z^2}[1 - (-1)^{l+l'}]$ in the right-hand side of (B.2), we arrive at the conclusion that the integrand becomes analytical after addition of terms with positive and negative values of M . Note that the eigenvectors and eigenvalues do not depend on the sign of M and the above consideration applies to the case $M = 0$. Consequently, one can evaluate (B.2) by residues choosing a branch of the complex-valued function $\sqrt{k_z^2 + q^2}$ arbitrarily.

The integrand of (B.2) has simple poles at $k_z = \pm i\sqrt{q^2 + 1/\lambda_{Mn}^2}$. Account of these poles leads to the following expression:

$$I = \frac{[\text{sgn}(z)]^{l+l'+m+m'} \lambda_{Mn} \exp\left[-\sqrt{1 + (q\lambda_{Mn})^2}|z|/\lambda_{Mn}\right]}{\sqrt{1 + (q\lambda_{Mn})^2}} \times d_{mM}^l[i\tau(q\lambda_{Mn})] d_{m'M}^{l'}[i\tau(q\lambda_{Mn})]. \quad (\text{B.6})$$

Substitution of (B.6) into (B.1) leads to an expression which is equivalent to (28).

We note that the integrand of (B.2) has another set of poles. Namely, these are poles of the functions $d_{mM}^l[\theta(k_z)]$ at $k_z = \pm iq$. These poles are of purely geometrical nature. We have calculated analytically the contributions of these poles to the Green's function to the few lowest orders in l, l' , and found that they cancel each other. However, we do not have a general proof of such cancellation to all orders. On the other hand, it is clear that if these poles could contribute to the plane-wave decomposition of the Green's function, the result would not satisfy the RTE since the matrix W is bounded and has no infinite eigenvalues. To confirm the validity of obtained analytical expression, we have computed I numerically by the fourth-order Simpson rule for a model set of parameters. Then we used this result to compute the Green's function for the particular case $\hat{\mathbf{s}} = \hat{\mathbf{s}}_0 = \hat{\mathbf{z}}$. The result coincided with the one predicted by formula (35) with machine accuracy in double precision.

References

- [1] M. C. W. van Rossum and Th. M. Nieuwenhuizen. Multiple scattering of classical waves: microscopy, mesoscopy and diffusion. *Rev. Mod. Phys.*, 71(1):313–371, 1999.
- [2] D. A. Boas, D. H. Brooks, E. L. Miller, C. A. DiMarzio, M. Kilmer, R. J. Gaudette, and Q. Zhang. Imaging the body with diffuse optical tomography. *IEEE Signal Proc. Mag.*, 18(6):57–75, 2001.
- [3] A. P. Gibson, J. C. Hebden, and S. R. Arridge. Recent advances in diffuse optical imaging. *Phys. Med. Biol.*, 50:R1–R43, 2005.
- [4] E. Amic, J. M. Luck, and Th. M. Nieuwenhuizen. Anisotropic multiple scattering in diffusive media. *J. Phys. A*, 29:4915–4955, 1996.
- [5] M. Firbank, S. R. Arridge, M. Schweiger, and D. T. Delpy. An investigation of light transport through scattering bodies with non-scattering regions. *Phys. Med. Biol.*, 41:767–783, 1996.
- [6] A. H. Hielscher, R. E. Alcouffe, and R. L. Barbour. Comparison of finite-difference transport and diffusion calculations for photon migration in homogeneous and heterogeneous tissues. *Phys. Med. Biol.*, 43:1285–1302, 1998.
- [7] A. D. Kim and J. B. Keller. Light propagation in biological tissue. *J. Opt. Soc. Am. A*, 20(1):92–98, 2003.
- [8] A. D. Kim. Transport theory for light propagation in biological tissues. *J. Opt. Soc. Am. A*, 21(5):820–827, 2004.
- [9] K. Ren, G. S. Abdoulaev, G. Bal, and A. H. Hielscher. Algorithm for solving the equation of radiative transfer in the frequency domain. *Opt. Lett.*, 29(6):578–560, 2004.
- [10] W. Cai, M. Lax, and R. R. Alfano. Analytical solution of the polarized photon transport equation in an infinite uniform medium using cumulant expansion. *Phys. Rev. E*, 63:016606, 2000.
- [11] M. Xu, W. Cai, M. Lax, and R. R. Alfano. Photon migration in turbid media using a cumulant approximation to radiative transfer. *Phys. Rev. E*, 65:066609, 2002.
- [12] D. W. Mueller and A. L. Crosbie. Three-dimensional radiative transfer in an anisotropically scattering, semi-infinite medium: generalized reflection function. *J. Quant. Spectrosc. Radiat. Transfer*, 74:43–68, 2002.
- [13] D. W. Mueller and A. L. Crosbie. Three-dimensional radiative transfer in an anisotropically scattering, plane-parallel medium: generalized reflection and transmission functions. *J. Quant. Spectrosc. Radiat. Transfer*, 75:661–721, 2002.
- [14] H. Jiang. Optical image reconstruction based on the third-order diffusion equation. *Opt. Express*, 4(8):241–246, 1999.

- [15] E. L. Hull and T. H. Foster. Steady-state reflectance spectroscopy in the p_3 approximation. *J. Opt. Soc. Am. A*, 18(3):584–599, 2001.
- [16] A. D. Klose, U. Netz, J. Beuthan, and A. H. Hielscher. Optical tomography using the time-independent equation of radiative transfer - Part 1: Forward model. *J. Quant. Spectrosc. Radiat. Transfer*, 72:691–713, 2002.
- [17] A. D. Klose and A. H. Hielscher. Optical tomography using the time-independent equation of radiative transfer - Part 2: Inverse model. *J. Quant. Spectrosc. Radiat. Transfer*, 72:715–732, 2002.
- [18] G. S. Abdoulaev and A. H. Hielscher. Three-dimensional optical tomography with the equation of radiative transfer. *J. Electron. Imag.*, 12(4):594–601, 2003.
- [19] W. Cai, M. Xu, and R. R. Alfano. Three-dimensional radiative transfer tomography for turbid media. *IEEE J. Selected Topics in Quantum Electronics*, 9(2):189–198, 2003.
- [20] G. E. Thomas and K. Stamnes. *Radiative transfer in the atmosphere and ocean*. Cambridge, 1999. [Chap. 8]
- [21] V. A. Markel. Modified spherical harmonics method for solving the radiative transport equation. *Waves in Random Media*, 14:L14–L19, 2004.
- [22] K. M. Case and P. F. Zweifel. *Linear transport theory*. Addison-Wesley, Reading, MA, 1967.
- [23] H. Barrett and K. J. Myers. *Foundations of image science*. Wiley Interscience, 2004. [Chap. 10.3.5]
- [24] D. A. Varshalovich, A. N. Moskalev, and V. K. Khersonskii. *Quantum theory of angular momentum*. World Scientific, Singapore, 1988.
- [25] H. G. Kaper. *Spectral methods in linear transport theory*. Birkhuser Verlag, Basel, 1982.
- [26] V. A. Markel and J. C. Schotland. Symmetries, inversion formulas and image reconstruction for optical tomography. *Phys. Rev. E*, 70(5):056616(19), 2004.
- [27] V. A. Markel and J. C. Schotland. Inverse problem in optical diffusion tomography. IV. Nonlinear inversion formulas. *J. Opt. Soc. Am. A*, 20(5):903–912, 2003.